The Cryosphere Discuss., 9, 4787–4843, 2015
www.the-cryosphere-discuss.net/9/4787/2015/
doi:10.5194/tcd-9-4787-2015

The Cryosphere Discussions
Open Access

Semi-automated calibration method for modelling of mountain permafrost evolution in Switzerland

A. Marmy[1], J. Rajczak[2], R. Delaloye[1], C. Hilbich[1], M. Hoelzle[1], S. Kotlarski[2], C. Lambiel[3], J. Noetzli[4], M. Phillips[5], N. Salzmann[1], B. Staub[1], and C. Hauck[1]

[1]Department of Geosciences, University of Fribourg, Fribourg, Switzerland
[2]Institute for Atmospheric and Climate Science, ETH Zurich, Switzerland
[3]Institute of Geography, University of Lausanne, Lausanne, Switzerland
[4]Department of Geography, University of Zurich, Zurich, Switzerland
[5]WSL, Swiss Federal Institute for Snow and Avalanche Research, Davos, Switzerland

Received: 11 July 2015 – Accepted: 4 August 2015 – Published: 10 September 2015

Correspondence to: A. Marmy (antoine.marmy@gmail.com)

Published by Copernicus Publications on behalf of the European Geosciences Union.

Abstract

Permafrost is a widespread phenomenon in the European Alps. Many important topics such as the future evolution of permafrost related to climate change and the detection of permafrost related to potential natural hazards sites are of major concern to our society. Numerical permafrost models are the only tools which facilitate the projection of the future evolution of permafrost. Due to the complexity of the processes involved and the heterogeneity of Alpine terrain, models must be carefully calibrated and results should be compared with observations at the site (borehole) scale. However, a large number of local point data are necessary to obtain a broad overview of the thermal evolution of mountain permafrost over a larger area, such as the Swiss Alps, and the site-specific model calibration of each point would be time-consuming. To face this issue, this paper presents a semi-automated calibration method using the Generalized Likelihood Uncertainty Estimation (GLUE) as implemented in a 1-D soil model (CoupModel) and applies it to six permafrost sites in the Swiss Alps prior to long-term permafrost evolution simulations. We show that this automated calibration method is able to accurately reproduce the main thermal condition characteristics with some limitations at sites with unique conditions such as 3-D air or water circulation, which have to be calibrated manually. The calibration obtained was used for RCM-based long-term simulations under the A1B climate scenario specifically downscaled at each borehole site. The projection shows general permafrost degradation with thawing at 10 m, even partially reaching 20 m depths until the end of the century, but with different timing among the sites. The degradation is more rapid at bedrock sites whereas ice-rich sites with a blocky surface cover showed a reduced sensitivity to climate change. The snow cover duration is expected to be reduced drastically (between −20 to −37 %) impacting the ground thermal regime. However, the uncertainty range of permafrost projections is large, resulting mainly from the broad range of input climate data from the different GCM-RCM chains of the ENSEMBLES data set.

1 Introduction

Permafrost is the thermal state of the subsurface that remains below 0 °C for two or more consecutive years (Harris et al., 2009). It occurs in the Arctic (Langer et al., 2013) and Antarctic ice-free regions (Vieira et al., 2010) as well as in mid-latitude mountain ranges such as in the European Alps (Boeckli et al., 2012), the Andes (Trombotto, 2000) and the Himalayan range (Weiming et al., 2012). In the last few decades, in the context of global warming, interest for permafrost has increased for various reasons such as greenhouse gas releases (e.g. Anthony et al., 2012), engineering and construction issues (e.g. Lepage and Doré, 2010; Bommer et al., 2010), water management issues (e.g. Quinton et al., 2011) and slope stability concerns (McColl, 2012). In mountain environments, the increase in air temperatures observed in the last decades (Mountain Research Initiative EDW, 2015) has had a notable effect on permafrost that are visible: (i) in the borehole data series by higher surface and subsurface ground temperatures and significantly deeper active layers (e.g. PERMOS, 2013) (ii) in geophysical data with a decrease of the electrical resistivities (Hilbich et al., 2008) and of seismic velocities (Hilbich, 2010) indicating a reduction of ice-content and (iii) in the increased activity of permafrost creep (Kääb and Kneisel, 2006; Barboux et al., 2013) and increased velocities of instable rock glaciers (Kääb et al., 2007; Gärtner-Roer, 2012).

Therefore, increasing effort has recently been put into permafrost modelling across different temporal and spatial scales. The spatial range of modelling approaches include: (i) 3-D models that can be used to simulate a limited number of processes such as heat conduction, latent heat and the effect of topography (e.g. Noetzli and Gruber, 2009; Noetzli et al., 2007) (ii) 2-D models (e.g. Etzelmüller et al., 2006; Hartikainen et al., 2010; Boeckli et al., 2012) that are applicable for permafrost distribution or zones of potential ground instability and (iii) 1-D models (e.g. Hipp et al., 2012; Westermann et al., 2011; Scherler et al., 2010; Luetschg et al., 2008) that are used to simulate many complex processes with a high number of feedback mechanisms. Recently, new

model approaches were developed which are able to simulate hydrological processes in 3-D, while keeping most thermal processes in 1d (Endrizzi et al., 2014). On hemispheric and global scales, 3-D land surface schemes are used to assess permafrost evolution. Here, ground temperatures are only calculated along 1-D soil columns on a hemispheric grid (e.g. Ekici et al., 2014, 2015; Chadburn et al., 2015) without lateral interaction.

The 3-D and 2-D approaches can be related more easily to geophysical or remote sensing methods, especially in Arctic lowlands where methane release is a major issue (Anisimov, 2007). In mountain environments, 1-dimensional modelling is widely used due to the spatial heterogeneity of surface and subsurface composition, topography, morphological landforms and microclimatic processes. Moreover, 1-D approaches are easier to relate to borehole temperature time series that are common in alpine permafrost research and are usually the only validation or calibration data available. However, the final goal of most permafrost modelling studies, especially in the Arctic (e.g. Ekici et al., 2015), is the representation of permafrost and permafrost processes in a distributed model. Whereas this is common in the arctic, this is still at a beginning stage in alpine environments due to many limiting factors, including the scarcity of input data, heterogeneity of surface, subsurface and microclimatical conditions. Fiddes et al. (2015) proposed a scheme that is leading in the direction of combining physically-based land surface models (LSMs) and gridded climate data to efficiently simulate air temperature and near-surface ground temperature but does not include borehole data validation.

Site-specific calibration is an important prerequisite for successful permafrost modelling with complex models. However the process of calibration often faces the scarcity of measured input parameters such as porosity, ice and water content, or thermal and hydraulic conductivities. All modelling approaches trying to model real conditions should use a certain specific procedure (Westermann et al., 2013) and some integrate more empirical calibration methods by manual tuning (Gruber and Hoelzle, 2001; Hipp et al., 2012; Scherler et al., 2013). With recent improvements in computing capacity,

the use of automated procedures of inverse modelling approaches using Monte-Carlo chains has become increasingly attractive (Jansson, 2012; Heerema et al., 2013), but so far this approach has not been tested in permafrost research.

The final goal of most permafrost modelling studies is their application to long-term climate impact simulations. Previous studies of combined climate-permafrost simulations with explicit subsurface simulations for the Alps are rare and were focused only on 1 or 2 sites (e.g. Engelhardt et al., 2010; Scherler et al., 2013) because of the limitations in the availability of ground temperature data and/or on-site meteorological data for calibration/validation purposes. Atmospheric forcing data for permafrost models can be derived from Global and/or Regional Climate Models (GCMs, RCMs). Especially for alpine terrain, RCMs offer an added value with respect to coarse resolution GCMs (e.g. Kendon et al., 2010; Torma et al., 2015) and are now widely used in scientific research, especially in the impact modelling community (e.g. Bosshard et al., 2014).

In this study, we present a semi-automated procedure for calibrating a soil model to a large number of points at different permafrost sites. The calibration procedure attempts to understand differences between the sites as well as to quantify the sensitivity of the soil model to the tested parameters. This method is a first step towards the realization of a well-calibrated distributed model, possibly done in the future by applying the semi-automated calibration method to all sites where surface or subsurface calibration data are available, and interpolating between with the help of additional data (e.g. Digital Elevation Models). The procedure has been applied to six test sites in the Swiss Alps: Stockhorn, Schilthorn, Muot da Barba Peider, Lapires, Murtèl-Corvatsch and Ritigraben. After calibration, the model set-up was used for long-term simulations driven by downscaled climate model data until the end of the 21st century, and an analysis of the evolution of the ground thermal regime and the snow cover is presented. The present work has two main objectives: (i) show the benefits and limitations of a semi-automated calibration procedure for detailed soil process modelling in permafrost terrain, use this procedure to identify differences and similarities among the test sites and to assess the

sensitivity of the soil model to certain parameters, and (ii) develop potential scenarios of the possible evolution of mountain permafrost in Switzerland.

2 Study sites

In the framework of the SNF-funded project "The Evolution of Mountain Permafrost of Switzerland" (TEMPS) (Hauck et al., 2013) and the Swiss permafrost monitoring network (PERMOS) (PERMOS, 2013), based on the collaboration of five research institutions, the necessary data sets for calibration and validation purposes were available for six different sites in the Swiss Alps. These sites cover a broad geographical range within Switzerland and represent a variety of landforms including rock slopes/plateaus, talus slopes and rock glaciers. The choice of the following sites was mainly driven by the availability of long-term time series of borehole temperatures and meteorological observations.

2.1 Schilthorn

The Schilthorn (SCH) massif (Bernese Alps, Switzerland) is situated at 2970 m a.s.l. (above sea level) in the north-central part of the Swiss Alps, and its non-vegetated lithology is dominated by deeply weathered dark limestone schists forming a surface layer of mainly sandy and gravelly debris up to several meters thickness over presumably strongly jointed bedrock. Within the framework of the European PACE project (Harris et al., 2003), the site was chosen for long-term permafrost observation and consequently integrated into the Swiss permafrost monitoring network PERMOS as one of its reference sites (PERMOS, 2013). The monitoring station at 2910 m a.s.l. is located on a small plateau on the north-facing slope and comprises a meteorological station (short and longwave radiation, air temperature, humidity, snow height, wind speed and direction) and three boreholes (14 m vertical, 100 m vertical and 100 m inclined) with continuous ground temperature measurements since

1999 (Vonder Mühll et al., 2000; Hoelzle and Gruber, 2008; Noetzli et al., 2008; Harris et al., 2009; PERMOS, 2013). Borehole data indicate permafrost of at least 100 m thickness, which is characterized by ice-poor conditions close to the melting point. Maximum active-layer depths recorded since the start of measurements in 1999 were generally around 4–5 m until the year 2008 but increasing to 6–7 m since 2009. During the superposition of very warm winter 2002/2003 with the summer heat wave 2003 (Schär et al., 2004) the active-layer depth increased exceptionally to 8.6 m, reflecting the potential for degradation of permafrost at this site (Hilbich et al., 2008).

The monitoring station is complemented by soil moisture measurements since 2007 and geophysical (mainly geoelectrical) monitoring since 1999 (Hauck, 2002; Hilbich et al., 2011). The snow cover at Schilthorn can reach maximum depths of about 2–3 m and usually lasts from October through to June/July. Due to its long time series and fairly homogeneous subsurface characteristics, the Schilthorn data-set was already used several times for long-term simulations but also in model sensitivity studies (Noetzli et al., 2008; Engelhardt et al., 2010; Scherler et al., 2010, 2013; Marmy et al., 2013; Ekici et al., 2015).

2.2 Murtèl-Corvatsch rock glacier

The rock glacier Murtèl-Corvatsch (COR) is situated in the Upper Engadine, Eastern Swiss Alps, and ranges from 2750 to 2600 m a.s.l., facing north-northwest. Its surface relief is pronounced with ogive-like structures with elevation differences between the furrows and ridges of up to 8 m. The surface consists of large blocks of up to several meters high which are composed by granodiorite and metamorphosed basalt of the Corvatsch nappe as well as muscovite and calcite marble of the Chastelets series (Schneider et al., 2013). Below this coarse blocky surface layer of approximately 3–3.5 m in thickness, a massive ice core (up to 90 %, Haeberli, 1990; Haeberli et al., 1998; Vonder Mühll and Haeberli, 1990) is present down to 28 m, with a frozen blocky layer below reaching from 28 to 50 m, probably adjacent to the bedrock (Arenson et al.,

2002). Borehole temperature data are available from 1987, which is the longest permafrost time series of the European Alps (PERMOS, 2013).

The main monitoring station is situated on a flat ridge at 2670 m a.s.l. and comprises a meteorological station (short- and long-wave radiation, air temperature, surface temperature, humidity, snow height, wind speed and direction) established in 1997 (Mittaz et al., 2000; Hoelzle et al., 2002; Hoelzle and Gruber, 2008) and two boreholes drilled in 1987 and 2000 (PERMOS, 2013). Permafrost temperatures are around −2 °C at 10 m depth and −1.4 °C at 25 m depth and the active layer has a thickness of 3.2 m on average. The comparison of the stratigraphy of the drill core of the 1987 borehole with the stratigraphies of the other core of the borehole located within a distance of 30 m shows significant small scale heterogeneities in the rock glacier (Vonder Mühll et al., 2001; Arenson et al., 2010). Permafrost conditions in the vicinity of the rock glacier are heterogeneous. Areas with fine grained subsurface material, vegetated soil and solid rock usually do not show any permafrost conditions, whereas coarse grained surface conditions often have permafrost conditions (Schneider et al., 2012, 2013; Scherler et al., 2014). Annual precipitation at the site is about 900 mm (982 mm St Moritz 1951–1980; 856 mm Piz Corvatsch 1984–1997). Typical maximum snow cover thickness is between 1 and 2 m. Mean annual air temperature is −1.7 °C for the observation period of March 1997 to March 2008 (Scherler et al., 2014). Geophysical monitoring (mainly ERT) has been conducted since 2005 (Hilbich et al., 2009).

2.3 Lapires

The Lapires (LAP) talus slope is located on the western slope of Val de Nendaz in Valais (46°06′ N, 7°17′ E) in the Western Swiss Alps, ranging from 2350 to 2700 m a.s.l. with a NNE orientation. Its surface consists of Gneiss schists and the talus shows a thickness of more than 40 m at the locations of the boreholes described below. Snow avalanches and minor rock falls with variable frequencies from one year to another affect the slope (Delaloye, 2004; Delaloye and Lambiel, 2005; Lambiel, 2006). The Lapires talus slope shows an active layer of about 4–5.5 m thickness situated on top

of an ice-rich (30–60 %) permafrost layer of around 15 m thickness with temperatures very close to the melting point (Scapozza et al., 2015; Staub et al., 2015).

The monitoring station consists of a meteorological station (air temperature and shortwave radiation since 1998, wind speed and direction and snow depths since 2009) installed in 1998 and three further boreholes installed in 2008 along a longitudinal profile (Scapozza et al., 2014). The site's Mean Annual Air Temperature (MAAT) was +0.5 °C at 2500 m a.s.l.

Compared to the strong microtopography of Murtèl rock glacier, the Lapires talus slope is comparatively homogeneous regarding slope and microtopography. The permafrost distribution within the talus slope is discontinuous (mainly related to heterogeneous substrate dominated by fine-grained material in the western part and coarse-blocky material in the eastern part) and linked to a complex system of internal air circulation also called the "chimney effect" (Delaloye and Lambiel, 2005). This air circulation is most effective when the temperature (and therefore density) gradient between the air and the voids in the porous substrate is significant, and it is responsible for ground cooling at the bottom of the talus slope, where cold air is suck up in winter. These 2-dimensional (or potentially 3-dimensional) processes cannot be explicitly simulated with the COUP-model (see also Staub et al., 2015), however, they have been confirmed by specific process modelling studies (Wicky, 2015).

2.4 Ritigraben

The active rock glacier Ritigraben (RIT) is located in the area Grächen-Seetalhorn (46°11′ N, 7°51′ E), Valais, western Swiss Alps, and covers an area between elevations of 2260 m to 2800 m a.s.l. Block sizes at the surface range from 0.5 up to several cubic meters. Active layer depth is almost constant at 4 m.

A 30 m borehole was drilled in 2002 in the lower part of the rock glacier at an altitude of 2615 m a.s.l. and was equipped with thermistors. Due to the movement of the rock glacier, the borehole is gradually being sheared off from the base upwards, and as a result temperature is currently only measured to a depth of 13 m. Borehole temperatures

indicate the formation of a seasonal talik between 11 and 13 m depth, which appears to be directly linked to snow melt water and rainfall infiltration (Zenklusen Mutter and Phillips, 2012). The effect of these processes on the thermal regime has recently been analysed by explicit process modelling using the model Snowpack (Luethi and Phillips, 2015).

The monitoring station is complemented by an automated weather station (net radiation, air temperature and relative humidity, surface temperature, snow depth, precipitation and wind speed and direction) installed in 2002 (Herz et al., 2003).

2.5 Muot da Barba Peider

The Muot da Barba Peider (MBP) talus slope is located near the top of the NW-oriented flank of the Muot da Barba Peider ridge at 2960 m a.s.l. above the village of Pontresina, Upper Engadine, Eastern Swiss Alps. The slope is 38° steep and is covered with coarse-blocks (Zenklusen et al., 2010). Two adjacent (50 m apart) boreholes were drilled in 1996 and are 18 m deep.

The drilling stratigraphy shows ground ice occurrences inside the talus, which reach a depth of about 4 m, with frozen bedrock below (Rist et al., 2006). Active layer depth varies between 1 and 2 m (Zenklusen et al., 2010). Due to the presence of experimental snow avalanche defence structures near borehole 1, the snow cover persists longer there in spring/summer and thus influences the ground thermal regime (Phillips, 2006).

Au automatic weather station was installed in 2003 and since then, MAAT is −3 °C. Precipitation is not measured on-site but mean annual regional values are around 1500 mm at this elevation (Zenklusen and Phillips, 2012). Maximum snow depths have ranged between 50 and 300 cm since 2003. The bedrock consists of gneiss from the upper Austroalpine nappe.

2.6 Stockhorn

The study site of the Stockhorn (STO) plateau is situated on an East–West oriented mountain crest around 3410 m a.s.l., to the west of the Stockhorn summit (3532 m a.s.l.) above Zermatt, Valais (45°59′ N 7°49′ E), Western Swiss Alps. The lithology consists of Albit–Muskowit schists and the surface is characterized by patterned ground that has developed in a thin debris cover. Significant amounts of ground ice could be observed in large ice-filled cracks during construction works of a new ski lift in summer 2007 (Hilbich, 2009). Two boreholes only 30 m apart were drilled in 2000 as part of the PACE project (Harris et al., 2003). The recorded borehole temperatures show that the Stockhorn plateau is strongly affected by 3-D topography effects (Gruber et al., 2004), because the 100 m deep borehole close to the north face exhibits significant colder temperatures than the 17 m deep borehole located close to the southern edge of the plateau. The monitoring station is complemented by a meteorological station (short- and long-wave radiation, air temperature, humidity, snow height, wind speed and direction) that was installed in 2002. A soil moisture station was added in 2014.

The MAAT at this site is −6.4 °C for 2002–2012 and the annual precipitation at 1500 mm (Gruber et al., 2004, based on King, 1990; Begert et al., 2003). This site is characterized by low precipitation and high solar radiation (mean short-wave incoming radiation from 2002–2013: 209.3 W m^{-2}) due to particular conditions created by surrounding mountain ranges exceeding 4000 m a.s.l. (Gruber et al., 2004).

3 Data and model

One of the main challenges in the modelling of permafrost evolution is the general lack of long (> 15 years) and gapless on-site multivariate meteorological data necessary as input for the calibration of the soil model. Similarly, data from GCM/RCM derived climate scenarios have to be downscaled and bias corrected for specific on-site conditions, which is non-trivial due to the high altitudes of most permafrost stations and the

above mentioned short length of on-site meteorological data. In this section we will explain the downscaling approach used, and introduce the available borehole data-sets used for calibration of the soil model. Finally, the physical basis of the COUP soil model as well as its major parameterizations will be explained.

3.1 Climate scenarios: statistical downscaling and bias correction

Site-specific climate scenarios have been developed for eight meteorological variables at daily resolution and for the period from 1951 to 2099. The scenarios are based on an ensemble of 14 regional climate model (RCM) projections from the EU ENSEMBLES project (van der Linden and Mitchell, 2009). It should be noted that, some variables have fewer GCM-RCM chains available: 7 for mean wind-speed and maximum wind-gusts and 13 for global radiation. Only the 13 chains with global radiation were used in the present study.

The ensemble accounts for a comprehensive range of model uncertainty and is forced by the IPCC SRES A1B emission scenario (Nakicenovic and Swart, 2000). Due to their limited spatial resolution, site-specific features are typically not resolved by climate models and even on resolved scales, models are subject to biases (e.g. Kotlarski et al., 2014). Statistical downscaling (SD) and bias correction (BC) techniques serve to attain representative conditions for the site scale and to remove model biases. SD/BC applications derive an empirical relationship between observations and model output. The established relationships are in turn used to translate long-term climate simulations to the site scale. Calibrating SD/BC techniques, however, requires long-term observations (e.g. 30 years and more), a prerequisite not met by the monitoring sites of the present study.

To obtain robust and reliable climate scenarios at the six considered sites, a newly implemented SD/BC method was used that specifically targets locations that lack long-term data. A detailed description and comprehensive validation of the approach is given by Rajczak et al. (2015). It is designed as a two-step procedure sketched in Fig. 1. In the first step, climate model simulations are downscaled to match long-term

observational measurements at a most representative site (MRS) within a surrounding measurement network (e.g. MeteoSwiss weather stations). In the second step, the downscaled and bias-corrected time series from the MRS are spatially transferred to the site of interest (e.g. a permafrost monitoring site). Both steps rely on the quantile mapping (QM) method, a well-established statistical downscaling and bias correction technique (e.g. Themessl, 2011). The concept behind QM is to correct the distribution of a given predictor (e.g. climate model output) in such a way that it matches the distribution of a predictand (e.g. observations of the same variable at a monitoring site). Values outside the range of calibrated values are treated using the correction for the 1st (99th) quantile. Within this study, the spatial transfer is performed from an objectively selected MRS within the MeteoSwiss monitoring network. Consequently, Rajczak et al. (2015) show that the MRS is, in many cases, not the closest station but rather one at a similar altitude.

3.1.1 Reconstruction of meteorological observations

The two-step procedure (Fig. 1) additionally facilitates the reconstruction of data at the monitoring site for non-measured periods. The concept behind reconstructing data is to spatially transfer (Fig. 1, step 2) observed values from an MRS to the target site. In the framework of the present study, data were reconstructed for some periods between 1981 and 2013. Note that reconstruction is constrained by the availability of data at the MRS. An extensive validation of the reconstruction performance is given by Rajczak et al. (2015).

3.1.2 Climate scenarios: projections of 2 m-temperature

Based on the developed site-scale scenarios, Fig. 2 provides the projected evolution of mean annual air temperature (MAAT) at 2 m above ground for the six considered sites in the period between 1961 and 2099. The projections assume an A1B emission scenario and include model uncertainty (i.e. range of estimates). While MAAT is predominantly

negative in the present-day climate, all six sites are subject to a significant increase in temperature and virtually all models agree at four of the six sites on positive mean temperatures by the end of the 21st century.

For each site, the reconstructed meteorological data used consists of daily series' for the period between 1981–2013 for five variables: mean air temperature, precipitation sum, mean wind speed, mean relative humidity and global radiation. For the site MBP, the global radiation series could not be reconstructed because of a lack of validation data. Therefore, this variable was not used as forcing variable in the calibration for this site and has been estimated by the model based on latitude and air temperature.

Despite the good quality of the reconstruction, some short gaps could not be avoided. These gaps have been filled by artificial random selection of data from other years at the same date. This method is satisfactory as the gaps are short and infrequent.

For seven of the chains, the wind speed scenarios were not available. As the wind plays only a minor role in the long-term trend of soil, it was satisfactory to use the median series of the seven other chains.

3.2 Borehole data

For calibration data, we used series of measured temperature data for each borehole with a minimum length of 10 years (Table 1). Borehole data is often considered as "ground truth data" but potential measurement errors cannot be excluded due to several reasons (such as sensor or logger drift, logger failure and infiltration of water inside the borehole casing, to name a few). Further, an unequal repartition of longer gaps may introduce a bias in the calibration. The gaps within the borehole temperature series have not been filled in order to avoid the introduction of inconsistency and additional errors in the data used for calibration. The periods with gaps are consequently ignored in the calibration process. In addition, one has to be aware that a level of uncertainty is introduced by calibrating the model only against temperature measurements and not against other sets of independent data such as snow depth, water content and/or apparent electrical resistivity.

3.3 COUP model description and experimental set-up

The model used for this study is the CoupModel, a 1-dimensional numerical model coupling the soil, snow and atmosphere processes (Jansson and Karlberg, 2004; Jansson, 2012). This model has already shown good aptitude to simulate mountain permafrost processes at Schilthorn (Engelhardt et al., 2010; Scherler et al., 2010, 2013; Marmy et al., 2013) and at Murtèl (Scherler et al., 2013, 2014). It also includes an optional procedure for semi-automatic calibration based on statistical indicators (see Sect. 4).

The model couples the water and heat transfer of the soil using the general heat flow equation:

$$\frac{\delta(CT)}{\delta t} - L_f \rho \frac{\delta \Theta_i}{\delta t} = \frac{\delta}{\delta z}\left(k \frac{\delta T}{dz}\right) - C_w T \frac{\delta q_w}{\delta z} - L_v \frac{\delta q_v}{\delta z} \quad (1)$$

where C ($J K^{-1}$) is the heat capacity of soil, C_w ($J K^{-1}$) is the heat capacity of water, T (K) is the soil temperature, L_f and L_v ($J kg^{-1}$) are the latent heat of freezing and vapor, ρ ($kg m^{-3}$) is the density, Θ_i is the volumetric ice content, k ($W m^{-1} K^{-1}$) is the thermal conductivity, t is the time, z is the depth and q_w and q_v ($kg m^{-2} s^{-1}$) are the water and vapor fluxes.

The lower boundary condition is derived from the sine variation of the temperature at the soil surface and a damping factor for the depth. If the lowest compartment is unsaturated, a percolation is calculated by gravitational forces.

Upper boundary conditions are calculated with a complete energy balance at the soil surface, or at the snow surface, if snow cover is present. The convective heat inflow of water is given by precipitation and snow melt multiplied by the surface temperature and the heat capacity of liquid water (C_w):

$$q_h(0) = \frac{T_s - T_1}{\Delta_z/2} + C_w(T_a - \Delta T_{Pa}) q_{in} + L_v q_w \quad (2)$$

where $q_h(0)$ ($J m^{-2} d^{-1}$) is the soil surface heat flow, T_s is the soil surface temperature, T_1 is the temperature in the uppermost soil layer, ΔT_{Pa} is a parameter representing the temperature difference between the air and the precipitation, q_{in} is the water infiltration rate, Δ_z is the depth change, q_w is the water vapour flow and L_v is the latent heat of vapor. For periods with snow cover, the upper boundary condition is calculated assuming steady state heat flow between the soil and a homogeneous snow pack using the thermal conductivity of snow. Patchy snow cover conditions can be parameterized with a critical snow height that corresponds to the snow height that completely covers the soil and is one of the most influencing parameters used later in the calibration procedure. The fraction of bare soil is then calculated by a ratio between 0 cm and this threshold (see Eq. 9). The fraction of snow free ground is then used to estimate the average soil surface temperature and the surface albedo.

Snow is simulated by CoupModel partitioning of the precipitation into rain and snow depending on temperature threshold parameters. The snow cover is assumed to be horizontally and vertically homogenous. The snow melt is estimated as part of the heat balance of the snow pack, including net radiation, sensible and latent heat flux to the atmosphere, heat flux in precipitation, snow temperature change and heat flux to the soil. Further important processes in COUP are listed in Table 2 together with the respective equations.

The soil structure consists of 18 to 25 compartments (depending on the site), with increasing thickness with depth, ranging from 0.1 m in the upper layers to 4 m in the lower layers (Fig. 3). The initial conditions are estimated by the model by using the first values of the meteorological data. To avoid imprecise initial conditions, the model is run from 1981 on, although the observational time series usually begin only around the year 2000. No additional spin up is needed as the model usually reaches the stable conditions (i.e. not influenced by initial conditions) after 10 to 15 years.

4 Calibration procedure: GLUE

With the recent increase in computing power, the automation of the calibration of soil models, also called inverse modelling, has been used increasingly (e.g. Finsterle et al., 2012; Cui et al., 2011; Boeckli et al., 2012; Tonkin et Doherty, 2009). This method can handle complex systems with a large number of free parameters and calibrate them against on-site measured data. Among the many statistical methods available, the Generalized Likelihood Uncertainty Estimation (GLUE), developed by Beven and Binley (1992), is implemented in the COUP model (Jansson, 2012) and has been used in the present study. GLUE assesses the equivalence of a large number of different parameter set-ups stochastically selected among a given set of parameter value ranges. It is based on the premise that any model set-up is, to a certain extent, in error with reality (Morton, 1993). Assigning a likelihood to any model set-up will allow the selection of the most correct one within the number of the tested set of model parameters. The probability of getting a reasonable likelihood increases with the number of simulations especially in a complex system with a large number of parameters. Moreover, expert knowledge of the system is required to select the parameters to test and to define their ranges to minimize the error sources resulting from physically intercorrelated parameters, autocorrelation, insensitive parameters and heteroscedasticity (sub-populations that have different variabilities from others invalidating statistical tests) in the residuals (Beven and Binley, 1992). However, a large number of simulations with different sets of parameters may also raise the equifinality problem; several model set-ups can lead to an acceptable calibration (Beven and Freer, 2001) which may lead to an uncertainty into the prediction. For example, two model set-ups giving the same likelihood during the calibration process could lead to different results when used for long-term simulations.

The aim of the calibration procedure is not to get a physical determination of the parameter values but to get a model that is thermally most representative of the ground thermal regime at a given site. Therefore, the value range of the tested parameters may

be beyond the values found in literature but this is necessary to report and compensate some imprecision and the incompleteness in the model structure as well as the underdetermination of other parameters.

In the present study, we selected 14 parameters that have no on-site measured value and that have either shown a large influence on modelled temperature variations in a preliminary analysis or are known to be important in reality. The 14 parameters (listed in the Table 2) were tested for each site in a first iteration of 50 000 simulations. Each of the simulations was run with different parameter values, selected stochastically, creating thus 50 000 different model set-ups. The most sensitive model parameters were then identified for each site based on their relative importance on the performances of calibration. Those four to six sensitive parameters were then used in a second iteration of 20 000 simulations to refine the calibration. It is important to note that, although the parameters tested and their ranges were equivalent for all the six sites, the sensitive parameters may differ from site to site depending on site-specific characteristics (see next section). From the 20 000 simulations of the second GLUE calibration iteration, five model set-ups for each site were then selected based on statistical performance indicators (r^2 and the mean error, ME) for ground temperature at several depths. The calibration procedure is summarized in Fig. 4. The calibration obtained by this method led to the selection of a model set-up, the closest to the optimum, for the long-term simulations forced by the GCM/RCM data.

5 Calibration results

5.1 Relative importance metrics

The GLUE method was used to test a large number of parameters at each site and to statistically assess their relative importance in the model. The relative importance of each parameter in the model is calculated based on the standardized covariance matrix of the tested parameters and related model performances using the LGM (Linde-

mann, Gold and Merenda) method (Lindeman et al., 1980) that averages the sequential sums of squares over all orderings of regressors. We group the parameters into six categories: (1) Snow parameters (T_{rain}, T_{snow}, $\rho_{snowmin}$, S_k, $Melt_{rad}$, $Melt_{temp}$, ΔS_{crit}), (2) Albedo parameters (α_{dry}, α_{wet}), (3) Hydraulic conductivity (k_w, g_m), (4) Porosity (Φ), (5) Thermal conductivity (K_{soil}) and (6) Evaporation (ψ_{eg}) and evaluate the influence of each parameter group on the statistical performance indicators r^2 and ME at three different depths (near-surface, around 10 m and the maximal depth of each borehole). The r^2 accounts for variance whereas ME accounts for absolute errors. The results are shown in Fig. 5 (left). Hereby, the relative importance of the six groups of parameters are shown for the three different depths as well as the absolute importance of the varying parameters on the simulations results (in %). A large relative importance identifies a parameter or process as being dominant with respect to the other parameter groups, however, it can still have a low overall importance on the simulation results, if the absolute importance is low.

As expected, Fig. 5 shows that the snow parameters have the greatest importance on the calibration performance for all sites. This importance is obviously pronounced at the surface, as the snow conditions are a large part of the upper boundary condition by influencing the ground surface temperature during the snow-covered period. The variation of the r^2 at the surface is explained by snow with a relative importance usually above 50 %, ranging from 34 % at RIT up to 72 % at COR and 90 % at LAP. These differences between the sites are explained by different snow conditions: there is a mean of about 280 days with snow cover per year at RIT whereas COR only has about 200 days of snow cover days per year, meaning that the more snow there is, the smaller its relative importance in the model. Hence a site with long and high snow cover is less sensitive to variations in the snow parameters (and therefore more difficult to calibrate), as the snow persists anyway during a long period, than sites with less snow and a faster transition between snow covered and snow-free ground. AT LAP, the snow cover conditions are unique because of the presence of ski tracks and frequent occurrence of avalanches (see Staub et al., 2015).

In comparison with the r^2, the ME is less influenced by snow parameters, as snow cover is less important in regards to the absolute surface temperatures than the temporal variation of temperature, i.e. by accurately reproducing the transition between snow-covered ground decoupled from atmosphere and snow-free ground. Interestingly, the relative influence of snow on ground temperatures is still large even at greater depths:, the snow explains 12 % of the r^2 and 10 % of the ME at MBP at 17.5 m; 65 % of the r^2 and 43 % of the ME at RIT at 30 m, 19 % of the r^2 and 54 % of the ME at SCH at 13.7 m; 8 % of the r^2 and 8 % of the ME at STO at 98.3 m. At 57.95 m at COR, the snow shows a very limited influence as it explains only 0.1 % of the r^2 and 0 % of the ME at this depth. This is probably related to the thick model layer with high porosity (62/43 %, cf. Fig. 3), where ice is permanently present due to negative temperatures. Such a thick ice layer decouples the lowest layers from processes of the upper boundary.

The albedo parameters have a significant influence on the calibration results at all sites, especially regarding temperature amplitudes at the surface with relative importance for the ME ranging from 17 % at SCH to 74 % at LAP. The r^2 (variability) is less or not influenced by the albedo. Indeed, the albedo effect only occurs during snow-free period, changing the amount of heat kept by the uppermost layer therefore influencing the absolute value of temperature but not really the inter-seasonal variation. In some cases at greater depths (r^2 and ME at 10 m at COR, 8 m at LAP), albedo appears to have a high relative influence, sometimes higher than its importance at the surface. This is most likely not related to physical processes in reality: those intermediate depths, which are located between the well calibrated upper and lower boundary conditions, are difficult to calibrate with any of the parameters tested (see the low percentages of absolute importance). Therefore, those values are interpreted as statistical artefacts.

The evaporation only has a very limited importance, with values between 0 and 10 % for all the sites. As an exception, RIT is sensitive to changes in evaporation as it influences both the r^2 and the ME values at the surface and at greater depth (up to 44 %).

The sum of the influence of snow parameters, albedo parameters and evaporation ranges from 58 (SCH) to 100 % (RIT) near the surface, from 26 % (COR) to 97 % (RIT) at medium depth and from 7 (STO) to 96 % (RIT) at larger depth for the r^2. This highlights the major role played by the upper boundary condition in the calibration. LAP and COR are exceptions as the importance of the upper boundary parameters is high at the surface (90 % for r^2 and 97 % for ME at LAP and 78 % for r^2 and 86 % of the ME at COR) but negligible at 19.6 m (LAP) and 57.95 m (COR). At this depth at LAP, the variation of the r^2 and the ME is mainly due to variation of the thermal conductivity. The model needs to broadly tune the thermal conductivities of certain layers (10–15 m) to correct the temperature at this depth where a missing process or an incorrect soil structure parameterization need to be corrected. LAP and COR are 2 ice-rich sites (as seen in the geophysical results Hilbich et al., 2009), with large blocks at the surface and high modelled porosity: the combination of these three effects decouples more the intermediate depths from the upper boundary conditions than at MBP and RIT, which are also talus slopes/rock glaciers, but with a smaller modelled porosity.

The thermal conductivity plays a large role at depth where its relative importance ranges from 34 % at SCH (ME, 13.6 m) to 89 % at STO (ME, 98.3) and, as mentioned before, 100 % at LAP (r^2 and ME at 19.6 m). COR shows a relatively small sensitivity of changes in the thermal conductivity (11 % of the ME at 57.95 m). At MBP, thermal conductivity plays a large role, even at the surface (67 % of the r^2). Only RIT is insensitive to changes in the thermal conductivity (3 % of ME at 30 m depth). At this site, opposed to the others, evaporation at the soil surface has a strong influence, even at depth. This is most likely due to 3-D advective water flow from the melting snow cover (Luethi and Phillips, 2015). Therefore, the evaporation parameter should to be adjusted during the calibration process in order to compensate the effect of lateral water circulation, a process that is not included in the model.

The calibration of the porosity and the hydraulic conductivity of different horizons show little or no influence on calibration performance. For the porosity, this is not surprising as the ranges tested are narrow to keep porosity close to reality. The only site

showing sensitivity of changes in porosity is MBP (20 % of importance for the r^2 at 10 m and 19 % at 17.5 m). This site is mostly sensitive to changes of the porosity of the 2nd soil layer (1.6 to 3.6 m depth). This could be due to an imprecise soil structure set-up that the model needs to correct.

When considering the absolute importance (% in Fig. 5, left), we notice that deep borehole (COR, RIT and STO) have low percentages, which is not surprising as the temperatures at those depths are less prone to variance and depend more on the structural set-up of the model. For all sites, the surface shows the highest sensitivity to the tested parameters mainly due, as explained above, to the high importance of snow and albedo parameters. At RIT, the r^2 at the surface is not easily calibrated with the current set-up, because the r^2 is relatively constant for all tested set-ups: as the temperature is very close to the surface (0.1 m), the meteorological forcing is the main driving factor for the r^2 at this depth. However, even if near-surface temperature variation depends mainly on the meteorological conditions, the ME can be tuned as some parameters (e.g. albedo, evaporation) are able to modify the energy balance at the surface. At several places (LAP, MBP) the absolute importance is low around 10 m and this is because this intermediate depth is harder to calibrate than the upper and the lower boundary conditions.

After the LGM analysis, the most sensitive parameters for each site were identified to be used in the second iteration of the GLUE calibration procedure (cf. Fig. 4) to refine the calibration focusing on sensitive parameters. The parameters listed in Fig. 5 (right), are the four to six most important parameters in the variation of statistical indicators; their relative importance for the variation of the r^2 and the ME at three different depths is represented by the pie charts. One parameter that shows high sensitivity is the ΔS_{crit} (threshold snow height for the snow to be considered as fully covered) which allows the model to correct for the imprecise snow conditions and systematic biases in the building of the snow cover. The biases regarding the disappearance of the snow cover in early summer are corrected by the parameter $\mathrm{Melt}_{\mathrm{rad}}$ (coefficient for the importance of global radiation in the melt function of the snow). The thermal conductivity (k_{soil}) is important

to adjust temperatures at middle and lower depth (COR, LAP, SCH and STO) but also at the surface (MBP). It can also be seen that snow parameters (blue colors in the pie diagrams) have stronger influence at the two bedrock sites (SCH, STO) compared with talus slopes and rock glaciers, where other processes such as advection, convection and latent heat processes (due to the higher ice content) play a major role at depth.

5.2 Ground temperatures

To identify the most accurate runs among the 20 000 runs of the second iteration, we apply a selection based on two balanced criteria: (i) selecting the runs with the highest r^2 (= seasonal and interannual variability) in layers close to the surface and (ii) reducing as much as possible the ME (= model temperature bias, leading to a globally too warm or too cold model) at greater depth. This option has been preferred over a globally best r^2 or ME averaged over all depths because this option would consider equally all depths whereas the surface is more important regarding decadal changes.

To address the potential problem of equifinality during long-term simulations (Sect. 6), we select an ensemble of five model set-ups giving similarly good calibration performances and analyzed whether they differ significantly regarding long-term simulation results and calibrated values. This analysis showed that we can exclude that the equifinality plays a major role in our study.

Figure 6a–c shows the performance of the calibration at each site, comparing the measured and the simulated temperatures at three different depths, also indicating the value of the r^2 and ME. It has to be pointed out that a low r^2 or high ME value does not mean that a better result at a certain depth cannot be obtained by GLUE, because this selection process is a compromise between r^2 and ME at several depths. Most calibration runs produce either well calibrated temperatures near the surface or at greater depths, but not both for the same set of calibration parameter.

The calibration at the surface is very good at LAP and STO with r^2 higher than 0.8, meaning that the upper boundary condition, especially the snow timing and duration could be well represented. At the four other sites, the r^2 at the surface ranges between

0.65 (COR) and 0.77 (MBP). The comparatively low values at COR are not surprising due to the presence of very coarse blocks (> 2 m) at the surface inducing additional processes in the active layer that influence the near-surface sensors in the borehole (cf. Scherler et al., 2014). The general variation and absolute values of near-surface ground temperature is satisfactory. Some systematic mismatches notwithstanding exist, such as insufficient cooling during winter at SCH and LAP, or excessive cooling in winter at MBP. At MBP, this is compensated by an equally high excessive warming during summer. At STO, the general behavior of the near-surface temperature is accurately reproduced by the calibration, but both the winter temperatures and the summer temperatures appear as smoothed (warmer in winter and cooler in summer). At COR, there is an insufficient warming in summer, leading to a negative bias at the surface.

Temperatures at or around 3 m are the most challenging to calibrate as the influences of the upper and the lower boundary conditions have to be balanced. Moreover, this depth is often within the seasonally thawing layer and the transition between the frozen and unfrozen conditions is difficult to reproduce, especially given that subsurface structure and composition is generally unknown. The selection process showed that the selection of the best r^2 at this depth led to the introduction of a strong positive bias in the absolute value (leading to disappearance of permafrost) and to poor calibration results at lower depth. This is why we put special emphasis on the reduction of the ME at this depth rather than having a high r^2 in order to be close to the mean annual ground temperatures. As a consequence, the seasonal variations at this depth could not always be reproduced. They are reproduced correctly only at MBP (low ME and high r^2) and, to a certain extent, at COR and SCH (cf. Fig. 6). At SCH a warm bias is introduced in the model at 3 m depth because of an insufficient cooling during winter. This bias is explained by the bias introduced at the upper boundary which propagates to larger depths. At COR, the warm bias at the surface in not reproduced at 3.55 m. At RIT and STO, the model shows a constant temperature at the freezing point, leading therefore to a large positive bias (1.74 K at RIT and 1.32 K at STO). At LAP, the model also shows temperatures at the freezing point at 3.6 m, and it is able to reproduce some

seasonal variations only at the end of the calibration period. The bias at LAP is slightly positive (0.25 K).

The calibration of the lowermost layer is always satisfactory even though the model shows a slight positive bias at STO (0.56 K), RIT (0.29 K) (probably originating from the propagation of the warm bias at 3 m) and MBP (0.28 K) and a negative bias at SCH (−0.25 K).

Even if the calibration resulting from the GLUE procedure is not always satisfactory, it represents the optimal set-up for the given initial model for each site under the constraints of this semi-automated calibration approach presented in this study.

6 Long-term simulations

One of the goals of any calibration is to get a suitable setoff model parameter to be used in further analysis. In TEMPS project, the overall goal is the investigation of the present and long-term evolution of mountain permafrost in Switzerland. Hence, we calibrated the model set-ups for each of the six sites as explained in the previous section to simulate the possible thermal evolution of permafrost until the end of the century. For this, the model was forced with the downscaled and bias corrected climate model output from 13 GCM/RCM chains as explained in Sect. 3.2. The corresponding changes of the two main meteorological driving variables air temperature (see Fig. 2) and precipitation are summarized in the Table 3.

Figure 7 shows the evolution of ground temperature at 10 and 20 m, both as mean of 13 scenario simulations for each site as well as the corresponding ensemble range. The chosen depths show permanently frozen conditions during the observation period (cf. also PERMOS 2013) but are subject to thaw in a climate warming perspective.

At all sites, the 10 m layer (Fig. 7a–c, top) is projected to be unfrozen by the end of the century, but there is a considerable difference regarding the timing between the sites. Moreover, there is uncertainty among the 13 different GCM/RCM chains (grey area in Fig. 7). The 10 m layer is projected to become unfrozen between the decades 2060

and 2090 at COR, 2030 and 2060 at LAP, 2020 and 2030 at SCH and 2010 to 2060 at STO. At RIT, it is projected to have seasonal positive temperatures at 10 m already from model year 2010 onwards, although the active layer is presently around 3 to 4 m deep in reality. This artefact comes from the positive bias introduced during calibration which is reproduced and enhanced when run with the climate model data. At MBP, the 10 m layer is projected to be unfrozen from around 2080 for certain chains but remains frozen until the end of the century for other chains. Once its ice has permanently melted, the 10 m layer is subject to undergo significant seasonal variations (see COR, RIT and STO). SCH is not as much affected by the seasonal variations although the layer is projected to be unfrozen early in the century because of a smaller decrease in snow cover duration in comparison with other sites. In addition, its permafrost degradation is less pronounced than projected in Scherler et al. (2013). This is most probably due to the cold bias introduced during the calibration and to a slightly higher porosity value at depth (7 % as opposed to 5 % in Scherler et al., 2013), leading to higher ice content and therefore a slower degradation. Note as well that the air temperature warming at SCH is the lowest (+3.36 K, see Table 3) compared to other sites.

At LAP and MBP, the soil is projected to still be frozen at 20 m at the end of the century (Fig. 7a–c, bottom). At COR, SCH and STO, some chains project a thawing, occurring around 2069 at COR, 2080 at SCH and 2085 at STO, while other chains project negative temperatures at 20 m until the end of the century.

As already mentioned, one key element for the evolution of the ground thermal regime is the snow cover duration. Its evolution in the future is expected to be mostly influenced by changes in air temperature: the changes in the annual sum of precipitation are highly uncertain and do not generally exceed ±5 % in the GCM/RCM output (see Table 3) (but with high variability among chains), while the simulated mean change in snow cover duration ranges from −20 % (SCH) to −37 % (LAP). Figure 8 shows the relationship between the air temperature warming and the decrease in snow cover duration. For all sites, the correlation is linear and the trend of snow cover duration decreases per degree of warming ranges from $-5.98\,\mathrm{d\,K^{-1}}$ (COR) to $-8.76\,\mathrm{d\,K^{-1}}$ (LAP).

This decrease represents a snow cover duration shortening of 48 days (COR) to 88 days (LAP) until the end of the century. The differences in the trend are due to site specific model set-up characteristics as the slope, the snow parameters (e.g. snow density) or differences in other meteorological variable (e.g. global radiation). The range of the different GCM/RCM chains is broad, confirming the high uncertainty and the general difficulty in predicting the evolution of precipitation.

7 Discussion

7.1 Approach

The GLUE calibration method is not meant to determine the physical values of a parameter. The model is realistic in the equations, but the values for all model parameter at all depths cannot be known and the GLUE method gives the ability of finding the value which gives the best fit with the observations within the number of tested runs. But as the system is complex, with sometimes highly uncertain initial and boundary conditions, non-linear processes and model structural errors make an optimum calibration impossible (Beven, 2002). It is therefore more relevant to analyze the residuals and the sensitivity to parameters than the values of the parameter themselves.

The calibration with GLUE depends on several subjective initial assumptions: (a) choice of tested parameters and their range: this choice has to be made by the modeler prior to the calibration and is a result of previous tests to identify relevant and sensitive parameters and, (b) the choice of criteria of acceptance. The results of the calibration would have been different with different assumptions. Moreover, the uncertainties of the calibration add themselves to the uncertainties of the observation and to the uncertainties of the climate models when considering the long-term simulations.

7.2 Calibration

One challenge of the calibration with GLUE is that there are many parameters to calibrate which are often underdetermined with respect to the available data. Therefore, the optimum is sometimes poorly-defined especially for sites that include processes like 2-D air circulation which is not taken into account in the present model formulation. According to Beven (2002), an increased physical realism of the model structure does not aid in obtaining a better calibration. The perfect model would include a semi-infinite number of parameters and be unique to each site, and this is of course unrealistic.

In comparison with other permafrost modelling studies (e.g. Scherler et al., 2013; Westermann et al., 2013; Fiddes et al., 2015), the calibration method reaches a satisfactory calibration level for most of the sites. The obtained biases in the calibration may originate from several phenomena (which are very likely linked): (a) the set of tested parameters missed one or several calibration parameter(s) that would have been sensitive regarding the calibration performances, (b) the ranges of the parameter tested were not large enough and did not allow the model to sufficiently use extreme values for certain parameters to compensate for a physical process that is not included in the model, (c) the number of runs was not sufficient to find the optimum for each site, (d) errors regarding the initial model structure (soil type, horizons, ...), (e) biases introduced in the reconstruction of the input meteorological data or (f) errors or imprecision in temperature measurements. Regarding point (b), we particularly think about convective flow of air or 2-D air or water circulation which is not included explicitly in the COUP model. In a previous study this was solved by artificially creating a heat source or sink to reproduce convection within the coarse blocky layer of rock glacier Murtèl (Scherler et al., 2013). A similar parameterization for advective water flow within the SNOWPACK model has been proposed by Luethi and Phillips (2015) for Ritigraben. In the present study, we focused on finding a semi-automated calibration method to simulate the long-term evolution at many sites. In this context, it would be unclear how these

processes (and the depths where they are active), and therefore the specifications of heat source/sinks, would evolve over time in a degrading permafrost.

Other processes not taken into account in the model concern the snow redistribution by avalanches or by wind that often takes place in high mountain environments (Hoelzle et al., 2001; Lehning et al., 2008; Mott et al., 2010). Snow has been shown to have a strong influence on the ground thermal regime both in field measurements and in the soil models because it is a boundary decoupling the atmosphere and the soil (e.g. Ling and Zhang, 2003; Zhang, 2005; Hoelzle and Gruber, 2008). In this study we could quantify the influence of several snow parameters. Snow has an especially strong influence at sites with shorter snow cover duration: there it is the most important parameter for the variations at the surface, but it also has a strong influence at deeper layers. The sites with a long-lasting snow cover (RIT and MBP) showed a reduced sensitivity to snow parameters as the snow is present most of the time and the transition between snow-covered and snow-free conditions is less difficult to simulate. This is in accordance with the analysis of Zhang (2005) who showed a strong influence of snow on permafrost, especially in warmer regions. The influence of snow has already been pointed out by many authors. In general, the definition of the upper boundary conditions (snow, albedo, evaporation) appears to be a crucial issue as they influence the performance of the calibration of the whole soil column.

Facing the scarcity of measured data, it is difficult to check whether the calibration obtained by the semi-automated procedure is robust for outputs other than temperature. However, there are possibilities to validate the calibration with electrical resistivity data (related to water/ice content) or direct soil moisture data but this is beyond the scope of this paper, especially as these data do not exist for all modelled sites. Efforts are currently being made in this direction on the site-level, with promising results of a joint calibration using temperature and electrical resistivity data at STO (Python, 2015). Efforts are also currently being made towards the installation a soil moisture network in mountain environments (SNF project SOMOMOUNT, provide again the P3-link). These data could serve as validation of the thermal calibration as shown for the

example of SCH (Fig. 9). Figure 9a and b show the soil moisture output of the model set-up giving the best fit with observed temperatures in comparison with on-site measured data (Fig. 9a and b) that stem from soil moisture sensors adjacent to the borehole (see Hilbich et al., 2011). Although some biases are present, like the absolute value of the maximal peak in early summer (about 10 % mismatch at 12 cm), the absolute minimum during winter (about 7 % mismatch at 12 cm), or the stable summer maximum at 60 cm, the general behavior is well reproduced: the mean values and the timing of freezing-thawing is satisfying. In a second step, we manually calibrated the parameter wilting point (soil water content which a plant dies, used in the water retention curve to define the minimal residual water). The wilting point is part of the water retention function and has notable influence on the freezing-point depression. By this the agreement with measured soil moisture was substantially improved (Fig. 9c and d) showing that model calibration can easily be further if additional data sets are available.

7.3 RCM-based simulations

Given the various sources of uncertainty mentioned above and the choice of only one emission scenario (A1B) in the climate simulations, the results of the long-term simulation should not be considered as a prediction but rather as a projection of the range of possible future evolution of permafrost in the Swiss Alps under a given scenario. Our long-term simulations showed that the permafrost evolution is more influenced by the specific regional climate scenario applied (i.e. *b* the specific GCM/RCM chain) than by differently calibrated CoupModel set-ups. Climate scenario uncertainty appears to be the dominant component of uncertainty in this study.

A similar climate impact study has been carried out by Scherler et al. (2013), but with a different calibration procedure of the CoupModel and a different RCM downscaling technique for SCH and COR. In comparison to their results for SCH, the timing of permafrost degradation at 10 m around 2020–2030 and the moment when the entire seasonal thaw layer cannot refreeze anymore in winter is modelled similarly, but the consecutive warming after the start of degradation is smaller in the present study.

Similarly, the 20 m layer shows a rapid degradation in Scherler et al. (2013) whereas it remains below the freezing point for most of the GCM/RCM chains in the present study. The discrepancies are mainly explained by a slightly different soil structure, which was part of the calibration approach in the present study. At COR, the results of Scherler et al. (2013) show slow warming at 10 m and at 20 m. In the present study, the warming is also slow but once the 10 m-layer is thawed, the warming propagates faster to deeper layers than in the results of Scherler et al. (2013). This difference is not surprising as Scherler et al. (2013) manually introduced a site-specific seasonal heat sink/source to compensate for the effect of air convection in the coarse blocky surface layer. By this, permafrost was conserved longer in the model than in a model set-up without parameterized convection. In addition, higher ice contents within the rock glacier ice core were simulated in Scherler et al. (2013) than in the present study (85 % vs. 62 %, cf. Fig. 3), which decelerates warming as well. On the contrary, the calibrated porosity values near the surface of the present study are higher (49 %) than in the previous study (10 %). Porosity values in heterogeneous rock glaciers are of course always highly uncertain, but it has to be noted that the best results of the GLUE procedure were not obtained with the highest porosities for the deeper layers: during the selection process, the consideration of the r^2 tended towards high porosities, but the best performances were obtained with lower porosities when considering the ME (cf. Fig. 3).

In contrast to Scherler et al. (2013), the structure of the model in the present study was not manually adapted to site-specific conditions, because the goal was to develop a calibration method that finds the model set-up with the best fit to observations in a semi-automated procedure. Therefore, the cooling of the ground by convection in the coarse blocky surface layer was only represented indirectly, leading to a probable overestimation of the warming at this site. However, it is not clear how the cooling by convection would evolve in a context of climate change and permafrost degradation.

At all six sites, significant permafrost degradation is projected, driven mostly by the projected increase in air temperature during snow-free periods and its prolongation in time due to snow cover decrease. This is in good agreement with earlier sensitiv-

ity studies using the same model (Marmy et al., 2013) and similar studies from other regions (Etzelmüller et al., 2011; Hipp et al., 2012). In general, the sites with blocky material and higher porosity (COR, LAP, MBP) show a lower sensitivity to climate change whereas the bedrock sites (SCH and STO) tend to have a more rapid degradation. At most places, a high porosity is coupled with higher interstitial ice contents, hence requiring more energy to melt the ice and warm the ground. As an exception, the simulated degradation at RIT is relatively fast despite a rather high porosity. This originates from two factors: (i) this site is projected to have one of the highest decreases in snow cover duration with −20.57 to −49.42 %, representing a period of −140 to −74 days per year and (ii) this site had the greatest warm bias at depth introduced during calibration which was responsible for the overestimation of degradation in the simulation results. The warm bias in the model was created because cooling by convection is not taken into account in the model (see COR) and because at this site a seasonal intra-permafrost talik has formed in the past years due to the infiltrating melt water from the snow cover (Luethi and Phillips, 2015). The calibration is forced to create unrealistic parameter settings as the model tries to reproduce those seasonal warm anomalies. At MBP, the degradation is projected to be slow compared to other sites. This reduced degradation does not originate from the bias in the calibration (cf. Fig. 6a), but may stem from the combination of various explanatory factors: (i) the mean air temperature warming is average (below +4 K), (ii) this reduced air temperature increase, coupled with the mean precipitation sum that is projected to increase for most of the GCM/RCM chains leads to a smaller decrease of the snow cover (mean: −22.81 %, i.e −48 days), therefore maintaining an efficient insulation layer decoupling the ground thermal regime from the atmosphere, (iii) one of the highest porosity of all the sites, and therefore a high interstitial ice content or (iv) one of the coldest initial ground thermal regimes, that could not be reproduced by the calibration.

Changes simulated in the snow cover duration are mostly influenced by the increasing air temperature and much less by change in mean annual precipitation sum. This is in agreement with Wang et al. (2014) who stated that the increase in atmospheric freez-

ing level is responsible for most changes in cryosphere in the future. Our CoupModel simulations showed a decrease of snow cover duration of about −20 to −37 %, which is in the same order of magnitude than the results by Bavay et al. (2009) who projected a mean reduction of snow cover duration of ca. 30–35 % for two alpine catchments (run under the B2 and A2 scenarios), and by Schmucki et al. (2014) who projected a decrease of snow cover of 32–35 % for high-elevation sites. During the next 10–20 years this reduction of snow cover may have an opposite effect to ground warming in summer: a decrease of the snow cover in fall and early winter can lead to a cooling of the ground, because the cool winter temperature can better penetrate the ground with no or reduced snow cover. However, sensitivity studies for a whole range of air temperature and precipitation changes suggest that until the end of the century the effect of warming is dominant over this potential cooling effect in late autumn/early winter (Marmy et al., 2013). In spring and late summer, the decrease of snow cover has always had a warming feedback because the snow is no longer present to isolate the ground from the positive summer temperatures.

The results of the long-term simulations have to be considered with caution as uncertainty may arise at several steps of the model chains: errors in the measurements used for calibration, structural errors of the model, choice of parameters and choice of their tested ranges, biases introduced during the calibration, emission scenario uncertainty or GCM/RCM chains uncertainty.

8 Conclusions

The present paper tested a semi-automated method for a soil/permafrost model calibration, in order to be able to use the method to calibrate a potentially large number of sites (e.g. in a distributed model). Other goals were to analyze of the sensitivity of the model results to certain parameters and to use the calibrated model set-ups for long-term RCM-based simulations of the permafrost evolution.

The following conclusions can be derived from the study:

- The method of semi-automated calibration using the Generalized Likelihood Uncertainty estimation (GLUE) showed an efficient ability to reproduce permafrost conditions at several permafrost sites in the Swiss Alps: the upper boundary conditions were simulated precisely and the absolute errors in the deepest layers were below a satisfactory error level. The r^2 at the surface ranged from 0.72 to 0.84 and the mean error at depth was usually smaller than 0.5 K except at STO and RIT.
- Some site-specific characteristics, such as vertical or 2-D circulation of air or lateral flows could not be reproduced by the method, hence leading to warm biases at depth.
- The method was generally suitable for large-scale or long-term modelling but is not recommended for site-specific process analysis, if there are existing dominant processes which are not included in the CoupModel formulation. In these cases, manual calibration and parameterization of the missing processes have to be added.
- The calibration of upper boundary parameters, especially parameters related to snow cover, were shown to have a large influence on the calibration performances, also on deeper ground layers. Therefore, efforts to obtain a precise upper boundary calibration must be undertaken, especially by increasing the length and the quality of surface measurements (GST, radiation, snow cover, etc.).
- The long-term simulations have shown a degradation trend at all sites, with an increasing active layer depth to at least 10 m at all sites until the end of the century, and even to 20 m at SCH and STO. However, strong uncertainty exists among the different GCM/RCM.
- The degradation is primarily driven by the change in air temperature during the snow-free period and the changing duration.

– The snow cover duration is projected to decrease of −20.03 to −37.06 % and is mainly driven by the change in air temperature.

We believe that the method presented here can be used as a starting point for large-scale modelling of the permafrost distribution in the Alps provided that an increased number of sites with high quality data series of observed ground temperature become available. A distributed model could be derived from the numerous calibrated sites by interpolation, in combination with digital elevation models, remote sensing data and subsurface data from geophysical surveys. As the model performance proved to be strongly influenced by the upper boundary condition, such a distributed model could also be generated from an interpolation between several GST measurements.

Acknowledgements. We would like to acknowledge the Swiss National Science Foundation for the funding of the TEMPS project (project no. CRSII2 136279) as well as the Swiss PERMOS network for the data provided. A special thank you to Per-Erik Jansson from Kungliga Tekniska Högskolan of Stockholm for the technical and scientific support with the CoupModel.

References

Anisimov, O. A.: Potential feedback of thawing permafrost to the global climate system through methane emission, Environ. Res. Lett., 2, 045016, doi:10.1088/1748-9326/2/4/045016, 2007.

Anthony, K. M. W., Anthony, P., Grosse, G., and Chanton, J.: Geologic methane seeps along boundaries of Arctic permafrost thaw and melting glaciers, Nat. Geosci., 5, 419–426, 2012.

Arenson, L. U., Hoelzle, M., and Springman, S.: Borehole deformation measurements and internal structure of some rock glaciers in Switzerland, Permafrost Periglac., 13, 117–135, 2002.

Arenson, L. U., Hauck, C., Hilbich, C., Seward, L., Yamamoto, Y., and Springman, S. M.: Subsurface heterogeneities in the Murtèl-Corvatsch rock glacier, Switzerland, in: Proceedings of the Sixth Canadian Permafrost Conference, Calgary, Alta, 12–16, 2010.

Barboux, C., Delaloye, R., Lambiel, C., Strozzi, T., Collet, C., and Raetzo, H.: Surveying the activity of permafrost landforms in the Valais Alps with InSAR, in: Mattertal – ein Tal in Bewegung, edited by: Graf, C., Publikation zur Jahrestagung der Schweizerischen Geomorphologischen Gesellschaft, 29, WSL, St Niklaus, Switzerland, 7–19, 2013.

Bavay, M., Lehning, M., Jonas, T., and Löwe, H.: Simulations of future snow cover and discharge in Alpine headwater catchments, Hydrol. Process., 23, 95–108, 2009.

Begert, M.: Homogenisierung von Klimamessreihen der Schweiz und Bestimmung der Normwerte 1961–1990: Schlussbericht des Projekts NORM90, MeteoSchweiz, Zürich, Switzerland, 2003.

Beven, K.: Towards a coherent philosophy for modelling the environment, P. Roy. Soc. Lond. A, 458, 2465–2484, 2002.

Beven, K. and Binley, A.: The future of distributed models: model calibration and uncertainty prediction, Hydrol. Process., 6, 279–298, 1992.

Beven, K. and Freer, J.: Equifinality, data assimilation, and uncertainty estimation in mechanistic modelling of complex environmental systems using the GLUE methodology, J. Hydrol., 249, 11–29, 2001.

Boeckli, L., Brenning, A., Gruber, S., and Noetzli, J.: A statistical approach to modelling permafrost distribution in the European Alps or similar mountain ranges, The Cryosphere, 6, 125–140, doi:10.5194/tc-6-125-2012, 2012.

Bosshard, T., Kotlarski, S., Zappa, M., and Schär, C.: Hydrological climate-impact projections for the Rhine river: GCM–RCM uncertainty and separate temperature and precipitation effects, J. Hydrometeorol., 15, 697–713, 2014.

Bommer, C., Phillips, M., and Arenson, L. U.: Practical recommendations for planning, constructing and maintaining infrastructure in mountain permafrost, Permafrost Periglac., 21, 97–104, 2010.

Chadburn, S., Burke, E., Essery, R., Boike, J., Langer, M., Heikenfeld, M., Cox, P., and Friedlingstein, P.: An improved representation of physical permafrost dynamics in the JULES land-surface model, Geosci. Model Dev., 8, 1493–1508, doi:10.5194/gmd-8-1493-2015, 2015.

Cui, T., Fox, C., and O'Sullivan, M. J.: Bayesian calibration of a large-scale geothermal reservoir model by a new adaptive delayed acceptance Metropolis Hastings algorithm, Water Resour. Res., 47, W10521, doi:10.1029/2010WR010352, 2011.

Delaloye, R.: Contribution à l'étude du pergélisol de montagne en zone marginale, PhD thesis, Université de Fribourg, Fribourg, 2004.

Delaloye, R. and Lambiel, C.: Evidence of winter ascending air circulation throughout talus slopes and rock glaciers situated in the lower belt of alpine discontinuous permafrost (Swiss Alps), Norsk Geogr. Tidsskr., 59, 194–203, 2005.

Ekici, A., Beer, C., Hagemann, S., Boike, J., Langer, M., and Hauck, C.: Simulating high-latitude permafrost regions by the JSBACH terrestrial ecosystem model, Geosci. Model Dev., 7, 631–647, doi:10.5194/gmd-7-631-2014, 2014.

Ekici, A., Chadburn, S., Chaudhary, N., Hajdu, L. H., Marmy, A., Peng, S., Boike, J., Burke, E., Friend, A. D., Hauck, C., Krinner, G., Langer, M., Miller, P. A., and Beer, C.: Site-level model intercomparison of high latitude and high altitude soil thermal dynamics in tundra and barren landscapes, The Cryosphere, 9, 1343–1361, doi:10.5194/tc-9-1343-2015, 2015.

Endrizzi, S., Gruber, S., Dall'Amico, M., and Rigon, R.: GEOtop 2.0: simulating the combined energy and water balance at and below the land surface accounting for soil freezing, snow cover and terrain effects, Geosci. Model Dev., 7, 2831–2857, doi:10.5194/gmd-7-2831-2014, 2014.

Engelhardt, M., Hauck, C., and Salzmann, N.: Influence of atmospheric forcing parameters on modelled mountain permafrost evolution, Meteorol. Z., 19, 491–500, 2010.

Etzelmüller, B., Heggem, E. S., Sharkhuu, N., Frauenfelder, R., Kääb, A., and Goulden, C: Mountain permafrost distribution modelling using a multi-criteria approach in the Hövsgöl area, northern Mongolia, Permafrost Periglac., 17, 91–104, 2006.

Etzelmüller, B., Schuler, T. V., Isaksen, K., Christiansen, H. H., Farbrot, H., and Benestad, R.: Modeling the temperature evolution of Svalbard permafrost during the 20th and 21st century, The Cryosphere, 5, 67–79, doi:10.5194/tc-5-67-2011, 2011.

Fiddes, J., Endrizzi, S., and Gruber, S.: Large-area land surface simulations in heterogeneous terrain driven by global data sets: application to mountain permafrost, The Cryosphere, 9, 411–426, doi:10.5194/tc-9-411-2015, 2015.

Finsterle, S., Sonnenthal, E. L., and Spycher, N.: Advances in subsurface modeling using the TOUGH suite of simulators, Comput. Geosci., 65, 2–12, 2012.

Gärtner-Roer, I.: Sediment transfer rates of two active rockglaciers in the Swiss Alps, Geomorphology, 167–168, 45–50, 2012.

Gruber, S. and Hoelzle, M.: Statistical modelling of mountain permafrost distribution: local calibration and incorporation of remotely sensed data, Permafrost Periglac., 12, 69–77, 2001.

Gruber, S., King, L., Kohl, T., Herz, T., Haeberli, W., and Hoelzle, M.: Interpretation of geothermal profiles perturbed by topography: the Alpine permafrost boreholes at Stockhorn Plateau, Switzerland, Permafrost Periglac., 15, 349–357, 2004.

Haeberli, W.: Pilot Analysis of Permafrost Cores from the Active Rock Glacier Murtèl I, Piz Corvatsch, Eastern Swiss Alps, Versuchsanstalt für Wasserbau, Hydrologie und Glaziologie ETH Zürich, 1990.

Haeberli, W., Hoelzle, M., Kääb, A., Keller, F., Vonder Mühll, D., and Wagner, S.: Ten years after drilling through the permafrost of the active rock glacier Murtèl, Eastern Swiss Alps: answered questions and new perspectives, in: Proceedings of the 7th International Conference on Permafrost, Yellowknife, Canada, Centre d'Etudes Nordiques, Université Laval, 1998.

Harris, C., Mühll, D. V., Isaksen, K., Haeberli, W., Sollid, J. L., King, L., Holmlund, P., Dramis, F., Guglielmin, M., and Palacios, D.: Warming permafrost in European mountains, Global Planet. Change, 39, 215–225, 2003.

Harris, C., Arenson, L. U., Christiansen, H. H., Etzelmüller, B., Frauenfelder, R., Gruber, S., Haeberli, W., Hauck, C., Hölzle, M., Humlum, O., Isaksen, K., Kääb, A., Kern-Lütschg, M., Lehning, M., Matsuoka, N., Murton, J. B., Nötzli, J., Phillips, M., Ross, N., Seppälä, M., Springman, S. M., and Vonder Mühll, D.: Permafrost and climate in Europe: monitoring and modelling thermal, geomorphological and geotechnical responses, Earth-Sci. Rev., 92, 117–171, 2009.

Hartikainen, J., Kouhia, R., and Wallroth, T.: Permafrost Simulations at Forsmark Using a Numerical 2-D Thermo-Hydro-Chemical Model, Svensk Kärnbränslehantering AB, Swedish Nuclear Fuel and Waste Management Company, Stockholm, 2010.

Hauck, C.: Frozen ground monitoring using DC resistivity tomography, Geophys. Res. Lett., 29, 2016, doi:10.1029/2002GL014995, 2002.

Hauck, C., Delaloye, R., Roer, I. H., Hilbich, C., Hoelzle, M., Kenner, R., Kotlarski, S., Lambiel, C., Marmy, A., Müller, J., Noetzli, J., Phillips, M., Rajczak, J., Salzmann, N., Schaepmann, M. E., Schär, C., Staub, B., and Völksch, I.: The evolution of mountain permafrost in Switzerland, AGU Fall Meeting Abstracts, 1, 4, 2013.

Heerema, K., Booij, M. J., Huting, R., Warmink, J. J., van Beek, E., and Jigjsuren, O.: Modelling impacts of climate change on the hydrology of a Mongolian catchment using an appropriate permafrost conceptualization, in: EGU General Assembly Conference Abstracts, 15, 4525, 2013.

Herz, T., King, L., and Gubler, H.: Thermal regime of coarse debris layers in the Ritigraben catchment, Matter valley, Swiss Alps, in: Eighth International Conference on Permafrost, Zürich, Extended Abstracts, 2013.
Hilbich, C.: Geophysical monitoring systems to assess and quantify ground ice evolution in mountain permafrost, PhD thesis, Univ., Jena, 2009.
Hilbich, C.: Time-lapse refraction seismic tomography for the detection of ground ice degradation, The Cryosphere, 4, 243–259, doi:10.5194/tc-4-243-2010, 2010.
Hilbich, C., Hauck, C., Hoelzle, M., Scherler, M., Schudel, L., Völksch, I., Vonder Mühll, D., and Mäusbacher, R.: Monitoring mountain permafrost evolution using electrical resistivity tomography: a 7 year study of seasonal, annual, and long-term variations at Schilthorn, Swiss Alps, J. Geophys. Res.-Earth, 113, F01S90, doi:10.1029/2007JF000799, 2008.
Hilbich, C., Marescot, L., Hauck, C., Loke, M. H., and Mäusbacher, R.: Applicability of electrical resistivity tomography monitoring to coarse blocky and ice-rich permafrost landforms, Permafrost Periglac., 20, 269–284, 2009.
Hilbich, C., Fuss, C., and Hauck, C.: Automated time-lapse ERT for improved process analysis and monitoring of frozen ground, Permafrost Periglac., 22, 306–319, 2011.
Hipp, T., Etzelmüller, B., Farbrot, H., Schuler, T. V., and Westermann, S.: Modelling borehole temperatures in Southern Norway – insights into permafrost dynamics during the 20th and 21st century, The Cryosphere, 6, 553–571, doi:10.5194/tc-6-553-2012, 2012.
Hoelzle, M. and Gruber, S.: Borehole and ground surface temperatures and their relationship to meteorological conditions in the Swiss Alps, in: Proceedings Ninth International Conference on Permafrost, 29 June–3 July 2008, Fairbanks, Alaska, 723–728, 2008.
Hoelzle, M., Mittaz, C., Etzelmüller, B., and Haeberli, W.: Surface energy fluxes and distribution models of permafrost in European mountain areas: an overview of current developments, Permafrost Periglac., 12, 53–68, 2001.
Hoelzle, M., Mühll, D. V., and Haeberli, W.: Thirty years of permafrost research in the Corvatsch–Furtschellas area, Eastern Swiss Alps: a review, Norsk Geogr. Tidsskr., 56, 137–145, 2002.
Jansson, P.-E.: CoupModel: model use, calibration and validation, T. ASABE, 55, 1335–1344, 2012.
Jansson, P.-E. and Karlberg, L.: Coupled heat and mass transfer model for soil-plant-atmosphere systems, Royal Institute of Technology, Dept. of Civil and Environmental Engineering, Stockholm, 2004.

Kääb, A. and Kneisel, C.: Permafrost creep within a recently deglaciated glacier forefield: Muragl, Swiss Alps, Permafrost Periglac., 17, 79–85, 2006.
Kääb, A., Frauenfelder, R., and Roer, I.: On the response of rockglacier creep to surface temperature increase, Global Planet. Change, 56, 172–187, 2007.
Kendon, E. J., Jones, R. G., Kjellström, E., and Murphy, J. M.: Using and designing GCM-RCM ensemble regional climate projections, J. Climate, 23, 6485–6503, 2010.
King, L.: Soil and rock temperatures in discontinuous permafrost: Gornergrat and Unterrothorn, Wallis, Swiss Alps, Permafrost Periglac., 1, 177–188, 1990.
Kotlarski, S., Keuler, K., Christensen, O. B., Colette, A., Déqué, M., Gobiet, A., Goergen, K., Jacob, D., Lüthi, D., van Meijgaard, E., Nikulin, G., Schär, C., Teichmann, C., Vautard, R., Warrach-Sagi, K., and Wulfmeyer, V.: Regional climate modeling on European scales: a joint standard evaluation of the EURO-CORDEX RCM ensemble, Geosci. Model Dev., 7, 1297–1333, doi:10.5194/gmd-7-1297-2014, 2014.
Lambiel, C.: Le pergélisol dans les terrains sédimentaires à forte déclivité: distribution, régime thermique et instabilités, UNIL-Faculté des géosciences et de l'environnement-Institut de géographie, Lausanne, Switzerland, 2006.
Langer, M., Westermann, S., Heikenfeld, M., Dorn, W., and Boike, J.: Satellite-based modeling of permafrost temperatures in a tundra lowland landscape, Remote Sens. Environ., 135, 12–24, 2013.
Lehning, M., Löwe, H., Ryser, M., and Raderschall, N.: Inhomogeneous precipitation distribution and snow transport in steep terrain, Water Resour. Res., 44, W07404, doi:10.1029/2007WR006545, 2008.
Lepage, J. M. and Doré, G.: Experimentation of mitigation techniques to reduce the effects of permafrost degradation on transportation infrastructures at Beaver Creek experimental road site, in: Proc. 63rd Canadian Geotechnical Conference, Calgary, Alberta, 2010.
Lindeman, R. H., Merenda, P. F., and Gold, R. Z.: Introduction to bivariate and multivariate analysis, Scott, Foresman, Glenview, IL, 1980.
Ling, F. and Zhang, T.: Impact of the timing and duration of seasonal snow cover on the active layer and permafrost in the Alaskan Arctic, Permafrost Periglac., 14, 141–150, 2003.
Luethi, R. and Phillips, M.: Talik formation in a rock glacier, Ritigraben, Grächen vs. Poster at TEMPS final symposium, Sion, Switzerland, 2015.
Luetschg, M., Lehning, M., and Haeberli, W.: A sensitivity study of factors influencing warm/thin permafrost in the Swiss Alps, J. Glaciol., 54, 696–704, 2008.

Marmy, A., Salzmann, N., Scherler, M., and Hauck, C.: Permafrost model sensitivity to seasonal climatic changes and extreme events in mountainous regions, Environ. Res. Lett., 8, 035048, doi:10.1088/1748-9326/8/3/035048, 2013.
McColl, S. T.: Paraglacial rock-slope stability, Geomorphology, 153, 1–16, 2012.
Mittaz, C., Hoelzle, M., and Haeberli, W.: First results and interpretation of energy-flux measurements over Alpine permafrost, Ann. Glaciol., 31, 275–280, 2000.
Morton, A.: Mathematical models: questions of trustworthiness, Brit. J. Philos. Sci., 44, 659–674, 1993.
Mott, R., Schirmer, M., Bavay, M., Grünewald, T., and Lehning, M.: Understanding snow-transport processes shaping the mountain snow-cover, The Cryosphere, 4, 545–559, doi:10.5194/tc-4-545-2010, 2010.
Mountain Research Initiative EDW Working Group: Elevation-dependent warming in mountain regions of the world, Nat. Clim. Change, 5, 424–430, 2015.
Nakicenovic, N. and Swart, R.: IPCC – Special Report on Emission Scenarios, Summary for Policy Makers, Cambridge University Press, 2000.
Noetzli, J. and Gruber, S.: Transient thermal effects in Alpine permafrost, The Cryosphere, 3, 85–99, doi:10.5194/tc-3-85-2009, 2009.
Noetzli, J., Gruber, S., Kohl, T., Salzmann, N., and Haeberli, W.: Three-dimensional distribution and evolution of permafrost temperatures in idealized high-mountain topography, J. Geophys. Res.-Earth, 112, F02S13, doi:10.1029/2006JF000545, 2007.
Noetzli, J., Hilbich, C., Hauck, C., Hoelzle, M., and Gruber, S.: Comparison of simulated 2-D temperature profiles with time-lapse electrical resistivity data at the Schilthorn crest, Switzerland, in: vol. 29, Ninth International Conference on Permafrost, University of Alaska, Fairbanks, 1293–1298, 2008.
PERMOS: Permafrost in Switzerland 2008/2009 and 2009/2010, edited by: Noetzli, J., Glaciological Report Permafrost No. 10/11 of the Cryospheric Commisson of the Swiss Academy of Sciences, Zurich, Switzerland, 80 pp., 2013.
Phillips, M.: Avalanche defence strategies and monitoring of two sites in mountain permafrost terrain, Pontresina, Eastern Swiss Alps, Nat. Hazards, 39, 353–379, 2006.
Python, S.: Technical Improvement of the 4-Phase Model to Better Assess the Ice, Water and Air Content Estimation in Permafrost Substrates, Master thesis, Department of Geosciences, University of Fribourg, Fribourg, Switzerland, 2015.

Quinton, W. L., Hayashi, M., and Chasmer, L. E.: Permafrost-thaw-induced land-cover change in the Canadian subarctic: implications for water resources, Hydrol. Process., 25, 152–158, 2011.
Rajczak, J., Kotlarski, S., Salzmann, N., and Schär, C.: Robust climate scenarios for sites with sparse observations: a two-step bias correction approach, Int. J. Climatol., doi:10.1002/joc.4417, in press, 2015.
Rist, A., Phillips, M., and Haeberli, W.: Influence of snow meltwater infiltration on active layer movement in steep alpine scree slopes within the discontinuous mountain permafrost, in: Proceedings, Asian Conference on Permafrost, edited by: Lai, Y., Ma, W., and Zhao, S., 10–11, 2006.
Scapozza, C., Lambiel, C., Bozzini, C., Mari, S., and Conedera, M.: Assessing the rock glacier kinematics on three different timescales: a case study from the southern Swiss Alps, Earth Surf. Proc. Land., 39, 2056–2069, 2014.
Scapozza, C., Baron, L., and Lambiel, C.: Borehole logging in Alpine periglacial talus slopes (Valais, Swiss Alps), Permafrost Periglac., 26, 67–83, 2015.
Schär, C., Vidale, P. L., Lüthi, D., Frei, C., Häberli, C., Liniger, M. A., and Appenzeller, C.: The role of increasing temperature variability in European summer heatwaves, Nature, 427, 332–336, 2004.
Scherler, M., Hauck, C., Hoelzle, M., Stähli, M., and Völksch, I.: Meltwater infiltration into the frozen active layer at an alpine permafrost site, Permafrost Periglac., 21, 325–334, 2010.
Scherler, M., Hauck, C., Hoelzle, M., and Salzmann, N.: Modeled sensitivity of two alpine permafrost sites to RCM-based climate scenarios, J. Geophys. Res.-Earth, 118, 780–794, 2013.
Scherler, M., Schneider, S., Hoelzle, M., and Hauck, C.: A two-sided approach to estimate heat transfer processes within the active layer of the Murtèl–Corvatsch rock glacier, Earth Surf. Dynam., 2, 141–154, doi:10.5194/esurf-2-141-2014, 2014.
Schmucki, E., Marty, C., Fierz, C., and Lehning, M.: Simulations of 21st century snow response to climate change in Switzerland from a set of RCMs, Int. J. Climatol., 35, 3262–3273, doi:10.1002/joc.4205, 2014.
Schneider, S., Hoelzle, M., and Hauck, C.: Influence of surface and subsurface heterogeneity on observed borehole temperatures at a mountain permafrost site in the Upper Engadine, Swiss Alps, The Cryosphere, 6, 517–531, doi:10.5194/tc-6-517-2012, 2012.

Schneider, S., Daengeli, S., Hauck, C., and Hoelzle, M.: A spatial and temporal analysis of different periglacial materials by using geoelectrical, seismic and borehole temperature data at Murtèl–Corvatsch, Upper Engadin, Swiss Alps, Geogr. Helv., 68, 265–280, 2013.

Staub, B., Marmy, A., Hauck, C., Hilbich, C., and Delaloye, R.: Ground temperature variations in a talus slope influenced by permafrost: a comparison of field observations and model simulations, Geogr. Helv., 70, 45–62, 2015.

Themessl, M. J., Gobiet, A., and Leuprecht, A.: Empirical-statistical downscaling and error correction of daily precipitation from regional climate models, Int. J. Climatol., 31, 1530–1544, doi:10.1002/joc.2168, 2011.

Tonkin, M. and Doherty, J.: Calibration-constrained Monte Carlo analysis of highly parameterized models using subspace techniques, Water Resour. Res., 45, W00B10, doi:10.1029/2007WR006678, 2009.

Torma, C., Giorgi, F., and Coppola, E.: Added value of regional climate modeling over areas characterized by complex terrain – precipitation over the Alps, J. Geophys. Res.-Atmos., 120, 3957–3972, doi:10.1002/2014JD022781, 2015.

Trombotto, D.: Survey of cryogenic processes, periglacial forms and permafrost conditions in South America, Revista do Instituto Geológico, 21, 33–55, 2000.

van der Linden, P. and Mitchell, J. F. B.: ENSEMBLES: Climate Change and its Impacts: Summary of Research and Results from the ENSEMBLES Project, Met Office Hadley Centre, Exter, UK, 2009.

Vieira, G., Bockheim, J., Guglielmin, M., Balks, M., Abramov, A. A., Boelhouwers, J., Cannone, N., Ganzert, L., Gilichinsky, A. A., Goryachkin, S., Lopez-Martinez, J., Meiklejohn, I., Raffi, R., Ramo, M., Schaefer, C., Serrano, E., Simas, F., Sletten, R., and Wagner, D.: Thermal state of permafrost and active-layer monitoring in the Antarctic: advances during the international polar year 2007–2009, Permafrost Periglac., 21, 182–197, 2010.

Vonder Mühll, D. and Haeberli, W.: Thermal characteristics of the permafrost within an active rock glacier (Murtèl/Corvatsch, Grisons, Swiss Alps), J. Glaciol., 36, 151–158, 1990.

Vonder Mühll, D. S., Hauck, C., and Lehmann, F.: Verification of geophysical models in Alpine permafrost using borehole information, Ann. Glaciol., 31, 300–306, 2000.

Vonder Mühll, D. S., Hauck, C., Gubler, H., McDonald, R., and Russill, N.: New geophysical methods of investigating the nature and distribution of mountain permafrost with special reference to radiometry techniques, Permafrost Periglac., 12, 27–38, 2001.

Wang, S., Zhang, M., Pepin, N. C., Li, Z., Sun, M., Huang, X., and Wang, Q.: Recent changes in freezing level heights in High Asia and their impact on glacier changes, J. Geophys. Res., 119, 1753–1765, 2014.

Weiming, C., Shangmin, Z., Chenghu, Z., and Xi, C.: Simulation of the decadal permafrost distribution on the Qinghai–Tibet Plateau (China) over the past 50 years, Permafrost Periglac., 23, 292–300, 2012.

Westermann, S., Boike, J., Langer, M., Schuler, T. V., and Etzelmüller, B.: Modeling the impact of wintertime rain events on the thermal regime of permafrost, The Cryosphere, 5, 945–959, doi:10.5194/tc-5-945-2011, 2011.

Westermann, S., Schuler, T. V., Gisnås, K., and Etzelmüller, B.: Transient thermal modeling of permafrost conditions in Southern Norway, The Cryosphere, 7, 719–739, doi:10.5194/tc-7-719-2013, 2013.

Wicky, J.: Numerische Modellierung von konvektiver Wärmeübertragung durch Luftflüsse in permafrostreichen Blockhalden, Master thesis, Department of Geosciences, University of Fribourg, Fribourg, Switzerland, 2015.

Zenklusen Mutter, E. and Phillips, M.: Active layer characteristics at ten borehole sites in alpine permafrost terrain, Switzerland, Permafrost Periglac., 23, 138–151, 2012.

Zenklusen Mutter, E., Blanchet, J., and Phillips, M.: Analysis of ground temperature trends in Alpine permafrost using generalized least squares, J. Geophys. Res.-Earth, 115, F04009, doi:10.1029/2009JF001648, 2010.

Zhang, T.: Influence of the seasonal snow cover on the ground thermal regime: an overview, Rev. Geophys., 43, RG4002, doi:10.1029/2004RG000157, 2005.

Table 1. Maximal depth, number of temperature sensors and series length of the boreholes used for calibration.

	Maximal depth (m)	Number of sensors	Series length
COR	57.95	53	Jul 1987–Feb 2013
LAP	19.6	19	Oct 1999–Dec 2012
MBP	17.5	10	Oct 1996–Jun 2011
RIT	25	10	Mar 2002–Sep 2012
SCH	13.7	17	Nov 1998–Jul 2013
STO	98.3	25	Oct 2002–Jun 2013

Table 2. List of parameters used in the GLUE calibration method and their corresponding equations.

Parameter	Description	Range tested	Equation(s) related
T_{rain}	Threshold temperature in the partition of precipitation into rain and snow. Above this value, precipitation falls only in liquid form.	0.1 to 4 (°C)	
T_{snow}	Threshold temperature in the partition of precipitation into rain and snow. Under this value, precipitation falls only in solid form.	−5 to 0 (°C)	$Q_p = \begin{cases} \min\left(1, (1-f_{liqmax}) + f_{liqmax}\frac{T_a - T_{snow}}{T_{snow}-T_{rain}}\right), & T_a \le T_{rain} \\ 0, & T_a > T_{rain} \end{cases}$
$\rho_{snowmin}$	Density of new snow. Used in the function determining the density of the whole snow pack (new and old snow).	50 to 200 (kg m^{-3})	$\rho_{snow} = \frac{\rho_{snowmin}}{119.17 f_{liqmax}}\left(67.92 + 51.25 e^{\frac{T_a}{2.59}}\right)$
S_k	Coefficient used in calculation of the thermal conductivity of snow	10^{-7} to 10^{-5}	$k_{snow} = S_k \rho_{snow}^2$
$Melt_{rad}$	Coefficient used to tune the importance of the global radiation on the empirical snow melt function	0 to 3×10^{-6}	$M_R = Melt_{rad}(1 + s_1(1 - e^{-s_2 2}))$
$Melt_{temp}$	Coefficient used to tune the importance of air temperatureon the empirical snow melt function	0.5 to 4	$Melt_{temp} = \begin{cases} Melt_{temp} & T_a \ge 0 \\ \frac{Melt_{temp}}{\Delta z_{snow} \rho_h} & T_a < 0 \end{cases}$ $M = Melt_{temp} T_a + Melt_{rad} R_{is} + \frac{r_{gh} a_h(0)}{L_f}$
ΔS_{crit}	Threshold snow height parameter for the soil to be considered as completely covered by snow. It is used to calculate the fraction of bare soil during patchy snow conditions by weighting the sum of temperature below the snow and the temperature of bare soil.	0.1 to 2 (m)	$f_{bare} = \begin{cases} \frac{\Delta z_{snow}}{\Delta S_{crit}} & \Delta z_{snow} < \Delta S_{crit} \\ 0 & \Delta z_{snow} \ge \Delta z_{cov} \end{cases}$
α_{dry}, α_{wet}	Albedo of dry/wet soil. This parameter is used to define the albedo function of the soil to calculate the net radiation.	10 to 40 (%)	$R_{snet} = R_{is}(1 - \alpha)$
ψ_{eg}	Factor to account for differences between water tension in the middle of top layer and actual vapour pressure at soil surface in the calculation of the energy balance at the soil surface.	0 to 3	$L_v = \frac{\rho_a c_p}{\gamma}\frac{(e_{surf} - e_a)}{r_{ae}}$ $e_{surf} = e_s(T_s) e^{\left(\frac{-\Psi_1 M_{water} g_{ncorr}}{R(T_s + T_{abszero})}\right)}$ $e_{corr} = 10^{(-\beta_{surf} \Psi_{eg})}$
k_w	Saturated hydraulic conductivity. This parameter is also used in the calculation of the unsaturated hydraulic conductivity.	100 to 10^5 (mm d^{-1})	$k_{tot} = k_w S_e^{\left(n+2+\frac{2}{\lambda}\right)}$
g_m	Empirical parameter used in the water retention function, in the effective saturation particularly.	0.1 to 2	$S_e = \frac{1}{(1+(\alpha\Psi)^{g_n})^{g_m}}$
Φ	Porosity, used in the water content calculation.	site-specific (%)	$\theta = S_e(\Phi - \theta_y) + \theta_r$
K_{soil}	Multiplicative scaling coefficient for the thermal conductivity applicable for each soil layer. This value is multiplied with the thermal conductivity calculated from the Kerten's equation for unfrozen and frozen soils.	−0.5 to 0.5	$k_{unfrozen} = h_1 + h_2\theta$ $k_{frozen} = b_1 10^{b_2 \rho_s} + b_3\left(\frac{\theta}{\rho_s}\right) 10^{b_4 \rho_s}$

Table 2. Continued.

Q_p:	thermal quality of precipitation (fraction of solid) (–)	e_s:	vapor pressure at saturation (mm water)
T_a:	air temperature (°C)	T_s:	soil surface temperature (°C)
F_{liqmax}:	maximal liquid water content fraction in precipitation (default = 0.5) (–)	Ψ_1:	water tension in the uppermost layer ($N m^{-1}$)
ρ_{snow}:	density of snow ($kg m^{-3}$)	M_{water}:	molar mass of water ($18.016 g mol^{-1}$)
k_{snow}:	thermal conductivity of snow ($W m^{-1} °C^{-1}$)	g:	gravity constant ($9.81 m s_2^{-1}$)
M_R:	melting of snow due to solar radiation ($kg J^{-1}$)	R:	gas constant ($8.31 J K^{-1} mol^{-1}$)
s_1, s_2:	empirical parameters (–)	$T_{abszero}$:	−273.15 °C
m_f:	coefficient to take the refreezing into account	δ_{surf}:	mass balance of water calculated at the surface (mm water)
Δz_{snow}:	snow depth (m)	k_{tot}:	total unsaturated hydraulic conductivity ($mm day^{-1}$)
M:	total snow melt ($mm day^{-1}$)	k_w:	saturated hydraulic conductivity ($mm day^{-1}$)
R_{is}:	global radiation ($MJ day^{-1}$)	S_e:	effective saturation (%)
F_{qh}:	scaling coefficient (–)	n and λ:	empirical parameters (–)
L_f:	latent heat of freezing ($J kg^{-1}$)	a, g_n and g_m:	empirical parameters (–)
F_{bare}:	fraction of bare soil	Ψ:	water tension ($N m^{-1}$)
R_{snet}:	is the short-wave radiation ($W m^{-2}$)	θ:	water content (%)
R_{is}:	global radiation ($W m^{-2}$)	θ_r:	residual water content (%)
α:	albedo (–)	θ_y:	threshold parameter for water tension (%)
ρ_a:	density of air ($kg m^{-3}$)	$k_{unfrozen}$:	thermal conductivity of unfrozen mineral soil ($W m^{-1} °C^{-1}$)
c_p:	heat capacity of air ($1.004 J g^{-1} K^{-1}$)	h_1, h_2:	empirical constants (–)
γ:	psychometer constant ($66 Pa K^{-1}$)	k_{frozen}:	thermal conductivity of frozen mineral soils ($W m^{-1} °C^{-1}$)
r_{as}:	aerodynamic resistance ($s m^{-1}$)	b_1, b_2, b_3, b_4:	empirical parameters (–)
e_{surf}:	vapor pressure at the soil surface (mm water)	ρ_s:	dry bulk soil density ($kg m^{-3}$)
e_a:	vapor pressure in air (mm water)		

Table 3. Summary of changes projected for two different decades (2040–2049 and 2090–2099): mean of 13 GCM/RCM chains for change in mean air temperature, in mean precipitation sum and in simulated snow cover duration (number of days per year with snow 0.1 m) compared to the 2000–2010 decade.

	Δ Air T (K)		Δ Prec (%)		Δ Days of snow (%)	
	2040–2049	2090–2099	2040–2049	2090–2099	2040–2049	2090–2099
Corvatsch	+1.58	+3.97	+8.4	+4.4	−10.84	−23.75
	+1.05/+2.11	+3.14/+5.38	+0.31/+18.18	−10.26/+16.43	−18.77/+6.74	−45.42/−4.91
Lapires	+1.67	+4.23	+0.63	−0.82	−16.73	−37.06
	+0.99/+2.15	+3.04/+5.83	−6.54/+9.28	−22.87–8.24	−23.67/−8.00	−57.28/−27.88
Muot da Barba Peider	+1.58	+3.95	+10.24	+6.74	−8.63	−22.81
	+1.05/+2.10	+3.13/5.33	+0.64/21.48	−8.79/+18.27	−11.94/−4.13	−37.11/−8.03
Ritigraben	+1.62	+4.10	+2.14	+4.89	−14.76	−32.31
	+0.97/2.08	+2.95/+5.65	−4.98/+11.64	−20.25/+14.68	−20.32/−5.93	−49.42/−20.57
Schilthorn	+1.40	+3.36	−1.20	−2.72	−9.21	−20.03
	+0.92/+1.91	+2.30/4.35	−8.50/+6.51	−16.78/+11.33	−12.24/−4.27	−35.73/−12.09
Stockhorn	+1.55	+3.86	+2.08	+4.68	−10.23	−24.59
	+0.96/+2.00	+2.84/+5.31	−5.61/+11.33	−20.01/+14.69	−14.18/−5.35	−39.53/−16.33

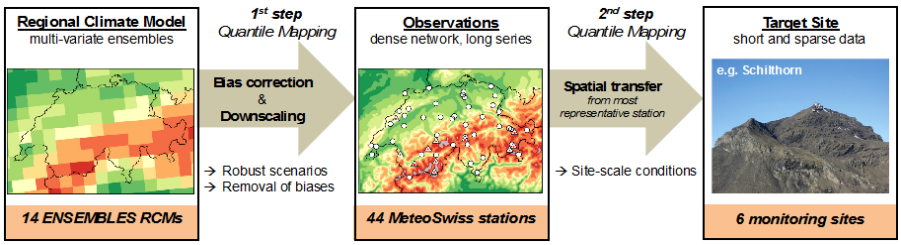

Figure 1. Schematics of the two-step procedure used for the generation of climate scenarios at the six monitoring sites. Figure adapted from Rajczak et al. (2015).

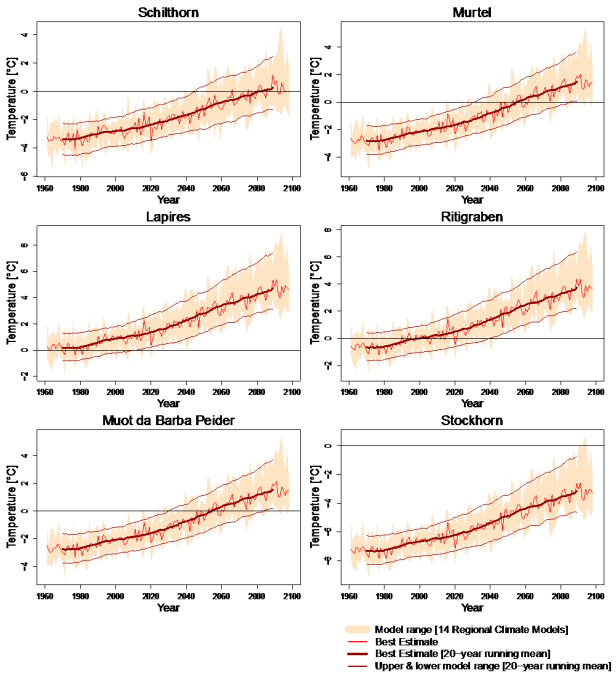

Figure 2. Site-scale climate scenarios of mean annual air temperature at 2 m above ground (MAAT) for the six considered permafrost monitoring sites. The results are based on the developed scenarios using the two-step procedure (Fig. 1) and are based on 14 ENSEMBLES regional climate models assuming an A1B greenhouse gas emission scenario.

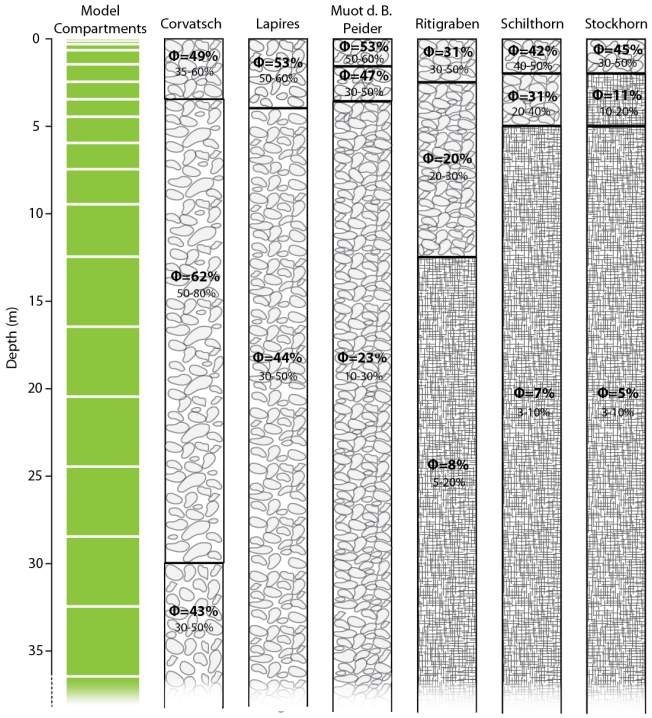

Figure 3. Description of the model layers as defined in the model (green) and of the simulated subsurface structure for each site. The depths of the horizons were estimated by experts, based on data from boreholes and geophysical surveys whereas the porosity Φ is defined by the GLUE calibration based on the ranges estimated by the experts (given below the GLUE estimated porosity values).

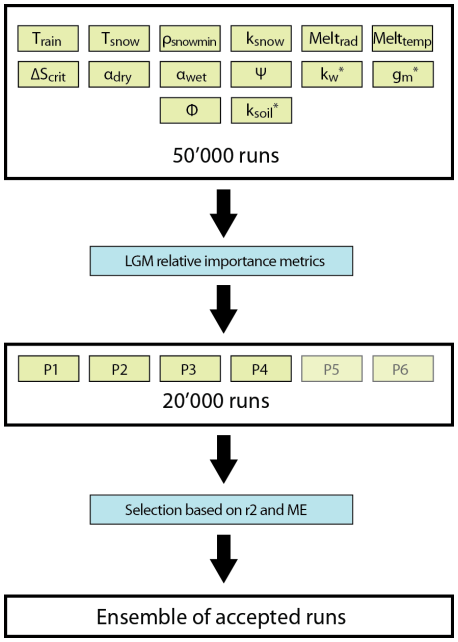

Figure 4. Calibration procedure using the GLUE method in the following steps: **(a)** 1st iteration, stochastically testing 14 different parameters in 50 000 runs, **(b)** selection of the most sensitive parameters for each site using the LGM method, **(c)** Refinement of the calibration with a second iteration of 20 000 runs focusing on the four to six sensitive parameters (may be different for each site), **(d)** selection of acceptable model set-ups among the 20 000 simulations based on statistical performance indicators (r^2 and the mean error, ME) for ground temperature at several depths. Among those four to six set-ups, the median (regarding the evolution of active layer thickness) is eventually used for long-term simulations.

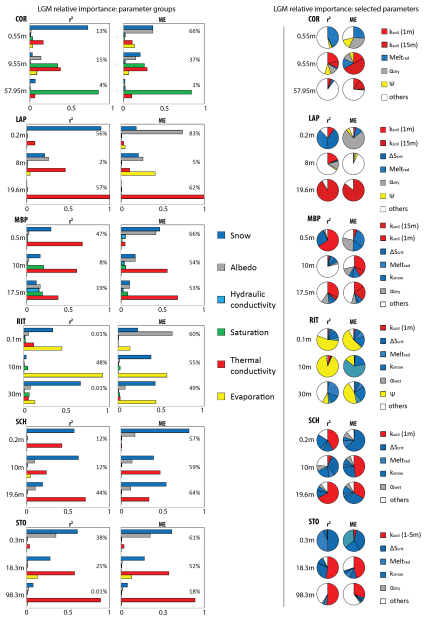

Figure 5. Left panels: LGM relative importance of six groups of parameters (snow, albedo, hydraulic conductivity, saturation, thermal conductivity and evaporation) on the r^2 (left panels) and the ME (right panels) at three different depths. The percentage indicates the total LGM absolute importance. Right panels: LGM relative importance of the most sensitive parameters that were selected for the second step of the calibration procedure.

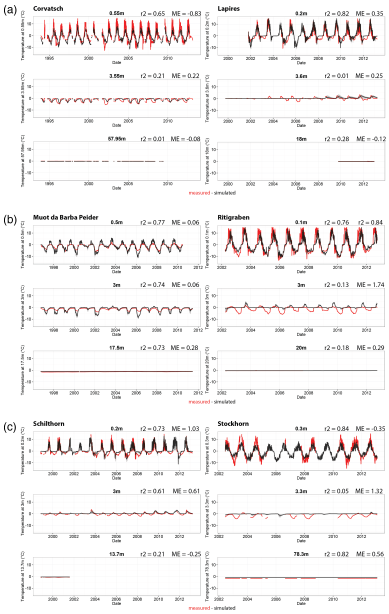

Figure 6. (a) Comparison of simulated (black) and measured (red) temperature during the calibration period at six sites at three different depths: one close to the surface, on around 3 m and one close to the lower boundary of the model for Corvatsch and Lapires. **(b)** Comparison of simulated (black) and measured (red) temperature during the calibration period at six sites at three different depths: one close to the surface, on around 3 m and one close to the lower boundary of the model for Muot da Barba Peider and Ritigraben. **(c)** Comparison of simulated (black) and measured (red) temperature during the calibration period at six sites at three different depths: one close to the surface, on around 3 m and one close to the lower boundary of the model for Schilthorn and Stockhorn.

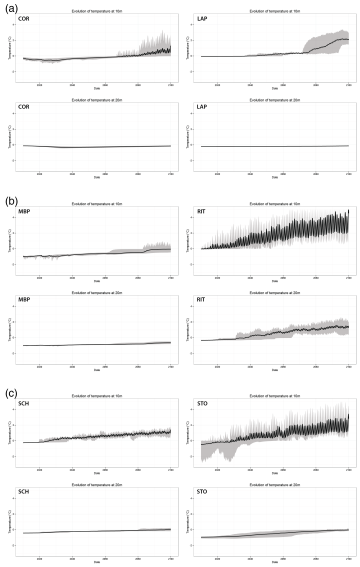

Figure 7. (a) Long-term evolution of ground temperatures at 10 m (top panels) and 20 m (bottom panels) as simulated with the COUP for Corvatsch (left panels) and Lapires (right panels). The black lines represent the median scenario and the grey zone the range of the 13 GCM/RCM chains. **(b)** Long-term evolution of ground temperatures at 10 m (top panels) and 20 m (bottom panels) as simulated with the COUP for Muot da Barba Peider (left panels) and Ritigraben (right panels). The black lines represent the median scenario and the grey zone the range of the 13 GCM/RCM chains. **(c)** Long-term evolution of ground temperatures at 10 m (top panels) and 20 m (bottom panels) as simulated with the COUP for Schilthorn (left panels) and Stockhorn (right panels). The black lines represent the median scenario and the grey zone the range of the 13 GCM/RCM chains.

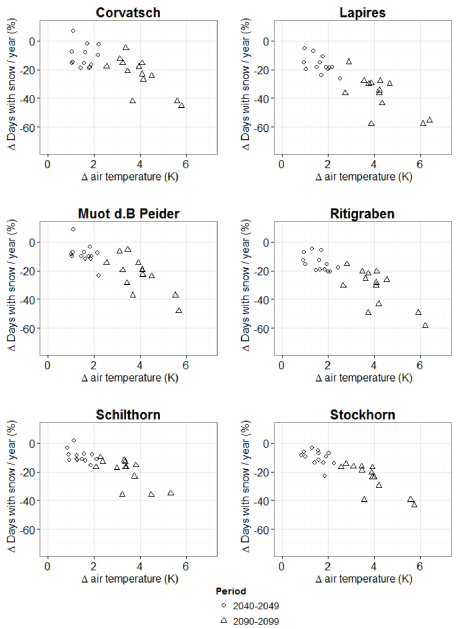

Figure 8. Relationship between the decreasing snow duration and the increase of air temperature for the decades 2040–2049 (dots, representing the 10 year means Δ for each GCM/RCM chain) and 2090–2099 (triangles, representing the 10 year means Δ for each GCM/RCM chain), in comparison with the decade 2000–2010. The trend is variable between the sites (from −5.29 to −8.76 % K^{-1}), but all sites shows a linear correlation between Δ air temperature and reduction of days with snow.

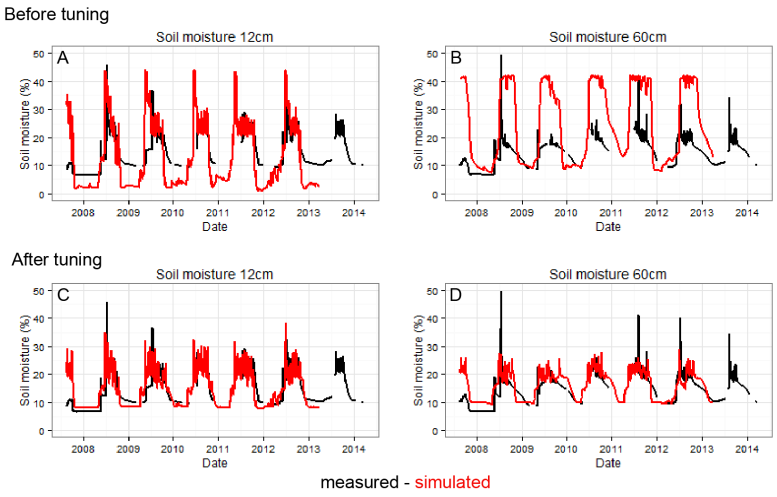

Figure 9. comparison of the simulated (red) and measured (black) soil moisture data at 12 cm (left panels) and 60 cm (right panels) at SCH. **(a)** and **(b)** are the results for soil moisture of the best thermal calibration while **(c)** and **(d)** are the results after a further calibration of the wilting point, showing that the calibration can be further improved with additional data sets.